Seismic attenuation due to wave-induced flow

S. R. Pride
Earth Sciences Division, Lawrence Berkeley National Laboratory, Berkeley, California, USA

J. G. Berryman
University of California, Lawrence Livermore National Laboratory, Livermore, California, USA

J. M. Harris
Department of Geophysics, Stanford University, Stanford, California, USA

Received 19 June 2003; revised 9 October 2003; accepted 23 October 2003; published 14 January 2004.

[1] Three P wave attenuation models for sedimentary rocks are given a unified theoretical treatment. Two of the models concern wave-induced flow due to heterogeneity in the elastic moduli at "mesoscopic" scales (scales greater than grain sizes but smaller than wavelengths). In the first model, the heterogeneity is due to lithological variations (e.g., mixtures of sands and clays) with a single fluid saturating all the pores. In the second model, a single uniform lithology is saturated in mesoscopic "patches" by two immiscible fluids (e.g., air and water). In the third model, the heterogeneity is at "microscopic" grain scales (broken grain contacts and/or microcracks in the grains), and the associated fluid response corresponds to "squirt flow." The model of squirt flow derived here reduces to proper limits as any of the fluid bulk modulus, crack porosity, and/or frequency is reduced to zero. It is shown that squirt flow is incapable of explaining the measured level of loss ($10^{-2} < Q^{-1} < 10^{-1}$) within the seismic band of frequencies ($1-10^4$ Hz); however, either of the two mesoscopic scale models easily produces enough attenuation to explain the field data. *INDEX TERMS:* 0935 Exploration Geophysics: Seismic methods (3025); 5102 Physical Properties of Rocks: Acoustic properties; 5114 Physical Properties of Rocks: Permeability and porosity; 5144 Physical Properties of Rocks: Wave attenuation; *KEYWORDS:* seismic attenuation, poroelasticity, seismic dispersion

Citation: Pride, S. R., J. G. Berryman, and J. M. Harris (2004), Seismic attenuation due to wave-induced flow, *J. Geophys. Res.*, *109*, B01201, doi:10.1029/2003JB002639.

1. Introduction

[2] The physics controlling the intrinsic seismic attenuation of sedimentary rock throughout the seismic band of frequencies (say 1 to 10^4 Hz) is still not entirely understood. In particular, seismic data from sedimentary regions often exhibits more intrinsic attenuation than can be explained using existing theoretical models. The principal goal of this paper is to provide models that can help explain the levels of loss determined from seismograms.

[3] Intrinsic loss is often quantified using the inverse quality factor Q^{-1} which represents the fraction of wave energy lost to heat in each wave period. For seismic transmission experiments (earthquake recordings, VSP, cross-well tomography, sonic logs), the total attenuation inferred from the seismograms can be decomposed as $Q_{\text{total}}^{-1} = Q_{\text{scat}}^{-1} + Q^{-1}$ where both the scattering and intrinsic contributions are necessarily positive. In transmission experiments, multiple scattering transfers energy from the coherent first-arrival pulse into the coda and into directions that will not be recorded on the seismogram, and is thus responsible for the effective "scattering attenuation" Q_{scat}^{-1}. Techniques have been developed that attempt to separate the intrinsic loss from the scattering loss in transmission experiments [e.g., *Wu and Aki*, 1988; *Sato and Fehler*, 1998]. In seismic reflection experiments, backscattered energy from the random heterogeneity can sometimes act to enhance the amplitude of the primary reflections. At the present time, techniques that can reliably separate the total inferred loss of a reflection experiment into scattering and intrinsic portions are generally not available.

[4] Cross-well experiments in horizontally stratified sediments produce negligible amounts of scattering loss so that essentially all apparent loss (except for easily corrected spherical spreading) is attributable to intrinsic attenuation. *Quan and Harris* [1997] use tomography to invert the amplitudes of cross-well P wave first arrivals to obtain the Q^{-1} for the layers of a stratified sequence of shaly sandstones and limestones (depths ranging from 500 to 900 m). The center frequency of their measurements is roughly 1750 Hz and they find that $10^{-2} < Q^{-1} < 10^{-1}$ for all the layers in the sequence. *Sams et al.* [1997] also measure the intrinsic loss in a stratified sequence of water-saturated sandstones, siltstones and limestones (depths ranging from 50 to 250 m) using

0148-0227/04/2003JB002639$09.00

VSP (30–280 Hz), cross-well (200–2300 Hz), sonic logs (8–24 kHz), and ultrasonic laboratory (500–900 kHz) measurements. *Sams et al.* [1997] calculate (with some inevitable uncertainty) that in the VSP experiments, $Q^{-1}/Q_{\text{scat}}^{-1} \approx 4$, while in the sonic experiments, $Q^{-1}/Q_{\text{scat}}^{-1} \approx 19$; that is, for this sequence of sediments, the intrinsic loss dominates the scattering loss at all frequencies. *Sams et al.* [1997] also find $10^{-2} < Q^{-1} < 10^{-1}$ across the seismic band.

[5] It will be demonstrated here that wave-induced fluid flow generates enough heat to explain these measured levels of intrinsic attenuation. Other attenuation mechanisms need not be considered since they are likely contributing much smaller percentages to the overall observed attenuation. The induced flow occurs at many different spatial scales that can broadly be categorized as "macroscopic," "mesoscopic," and "microscopic."

[6] The macroscopic flow is the wavelength-scale equilibration occurring between the peaks and troughs of a *P* wave. This mechanism was first treated by *Biot* [1956a, 1956b] and is often simply called "Biot loss." However, the flow at such macroscales drastically underestimates the measured loss in the seismic band (by as much as 5 orders of magnitude). Two possible alternatives to Biot loss were therefore proposed in the mid-1970s.

[7] First, *Mavko and Nur* [1975, 1979], *Budiansky and O'Connell* [1976], and *O'Connell and Budiansky* [1977] proposed a microscopic mechanism due to microcracks in the grains and/or broken grain contacts. When a seismic wave squeezes a rock having such grain-scale damage, the cracks respond with a greater fluid pressure than the main pore space resulting in a flow from crack to pore that *Mavko and Nur* [1975] named "squirt flow". *Dvorkin et al.* [1995] have also presented a squirt flow model applicable to liquid-saturated rocks. Although squirt flow seems capable of explaining much of the measured attenuation in the laboratory at ultrasonic frequencies and may also turn out to be important for propagation in ocean sediments at ultrasonic frequencies [*Williams et al.*, 2002], we show here that this mechanism cannot explain the attenuation in the seismic band.

[8] Second, *White* [1975] and *White et al.* [1975] modeled the wave-induced flow created by mesoscopic-scale heterogeneity. Mesoscopic length scales are those larger than grain sizes but smaller than wavelengths. Heterogeneity across these scales may be due to lithological variations or to patches of different immiscible fluids. When a compressional wave squeezes a material containing mesoscopic heterogeneity, the effect is similar to squirt with the more compliant portions of the material responding with a greater fluid pressure than the stiffer portions. There is a subsequent flow of fluid capable of generating significant loss in the seismic band.

[9] *White* [1975] considered the flow in a concentric porous sphere model in which the inner sphere is saturated by one fluid type (say gas), the outer shell is saturated by another fluid type (say liquid), and the porous frame properties are everywhere uniform. This is the first so-called "patchy saturation" model. White had the insight to use the *Biot* [1956a, 1956b] theory as the local model for the mesoscopic flow between the spheres. *Dutta and Odé* [1979a, 1979b] and *Dutta and Seriff* [1979] went on to make several important corrections to the initial *White* [1975] model, adding to our understanding of the low-frequency and high-frequency limits. *White*'s [1975] prediction of enhanced attenuation in the presence of even small volume fractions of gas phase has been experimentally confirmed [e.g., *Murphy*, 1982, 1984; *Cadoret et al.*, 1998].

[10] *White et al.* [1975] considered the wave-induced flow between the mesoscopic-scale layers in a sedimentary basin. Here the mesoscopic heterogeneity is in the frame properties of the porous rocks with a single fluid saturating all layers. Again, Biot theory was used as the local model for the mesoscopic flow. A host of theoretical refinements have subsequently been added to White's initial model of mesoscopic flow in finely layered media [e.g., *Norris*, 1993; *Gurevich and Lopatnikov*, 1995; *Gelinsky and Shapiro*, 1997].

[11] More recent work by *Johnson* [2001] has treated wave-induced mesoscopic flow due to patchy saturation without placing restrictions on the patch geometries. The present study also seeks to model the wave-induced flow for arbitrary mesoscopic geometry due either to lithological variations or to patchy saturation, albeit under the restriction that only two porous phases are mixed together in each averaging volume. Furthermore, our same formalism is shown to produce new exact results at both low and high frequencies for the *Dvorkin et al.* [1995] squirt flow model.

[12] In section 2, we review the recent theory of *Pride and Berryman* [2003a, 2003b] treating the mesoscopic loss created by lithological patches having, for example, different degrees of consolidation. This so-called "double-porosity" model provides the theoretical framework that will be used throughout. In section 3, we reanalyze the patchy saturation model of *Johnson* [2001] and demonstrate numerically that our double-porosity approach to the problem is asymptotically identical to Johnson's result in the limits of low and high frequencies (both analyses are exact for the model in the two limits). In section 4, we provide a new analysis of the *Dvorkin et al.* [1995] squirt flow model that is numerically compared to the approximate analysis of *Dvorkin et al.* [1995]. Finally, in the concluding section 5, we summarize what has been learned from these models.

2. Review of the Double-Porosity Theory

[13] In this theory, the mesoscopic heterogeneity is modeled as a mixture of two porous phases saturated by a single fluid.

[14] Various scenarios can be envisioned for how two porous phases might come to reside within a single geological sample. For example, even within an apparently uniform sandstone formation, there can remain a small volume fraction of less consolidated (even noncemented) sand grains. This is because diagenesis is a transport process sensitive to even subtle heterogeneity in the initial grain pack resulting in spatially variable mineral deposition [e.g., *Thompson et al.*, 1987] and, supposedly, in spatially variable elastic moduli. Alternatively, the two phases might correspond to interwoven lenses of detrital sands and clays; however, any associated anisotropy in the deviatoric seismic response will not be modeled in the present paper. Jointed rock is also reasonably modeled as a double-porosity

material. The joints or macroscopic fractures are typically more compressible and have a higher intrinsic permeability than the background host rock they reside within.

2.1. Local Governing Equations

[15] Each porous phase is locally modeled as a porous continuum and obeys the laws of poroelasticity [e.g., *Biot*, 1962]

$$\nabla \cdot \boldsymbol{\tau}_i^D - \nabla p_{ci} = \rho \ddot{\mathbf{u}}_i + \rho_f \dot{\mathbf{Q}}_i, \tag{1}$$

$$\mathbf{Q}_i = -\frac{k_i}{\eta}\left(\nabla p_{fi} + \rho_f \ddot{\mathbf{u}}_i\right), \tag{2}$$

$$\begin{bmatrix} \nabla \cdot \dot{\mathbf{u}}_i \\ \nabla \cdot \mathbf{Q}_i \end{bmatrix} = -\frac{1}{K_i^d}\begin{bmatrix} 1 & -\alpha_i \\ -\alpha_i & \alpha_i/B_i \end{bmatrix}\begin{bmatrix} \dot{p}_{ci} \\ \dot{p}_{fi} \end{bmatrix}, \tag{3}$$

$$\boldsymbol{\tau}_i^D = G_i\left(\nabla \mathbf{u}_i + \nabla \mathbf{u}_i^T - \frac{2}{3}\nabla \cdot \mathbf{u}_i \mathbf{I}\right), \tag{4}$$

where the index i represents the two phases (i = 1, 2). The response fields in these equations are themselves local volume averages taken over a scale larger than the grain sizes but smaller than the mesoscopic extent of either phase. The local fields are: $\mathbf{u}_i$, the average displacement of the framework of grains; $\mathbf{Q}_i$, the Darcy filtration velocity; p_{fi}, the fluid pressure; p_{ci}, the confining pressure (total average pressure); and $\boldsymbol{\tau}_i^D$, the deviatoric (or shear) stress tensor. In the linear theory of interest here, the overdots on these fields denote a partial time derivative. In the local Darcy law (2), η is the fluid viscosity and the permeability k_i is a linear time convolution operator whose Fourier transform $k_i(\omega)$ is called the "dynamic permeability" and can be modeled using the theory of *Johnson et al.* [1987] (see Appendix A).

[16] In the local compressibility law (3), K_i^d is the drained bulk modulus of phase i (confining pressure change divided by sample dilatation under conditions where the fluid pressure does not change), B_i is *Skempton*'s [1954] coefficient of phase i (fluid pressure change divided by confining pressure change for a sealed sample), and α_i is the *Biot and Willis* [1957] coefficient of phase i defined as

$$\alpha_i = (1 - K_i^d/K_i^u)/B_i, \tag{5}$$

where K_i^u is the undrained bulk modulus (confining pressure change divided by sample dilatation for a sealed sample). In the present work, no restrictions to single-mineral isotropic grains will be made. Finally, in the deviatoric constitutive law (4), G_i is the shear modulus of the framework of grains. At the local level, all these poroelastic constants are taken to be real constants. In Appendix A we give the *Gassmann* [1951] fluid substitution relations that allow B_i and α_i to be expressed in terms of the porosity ϕ_i, the fluid and solid bulk moduli K_f and K_s, and the drained modulus K_i^d.

2.2. Double-Porosity Governing Equations

[17] In the double-porosity theory, the goal is to determine the average fluid response in each of the porous phases in addition to the average displacement of the solid grains [*Berryman and Wang*, 1995]. The averages are taken over regions large enough to significantly represent both porous phases, but smaller than wavelengths. Assuming an $e^{-i\omega t}$ time dependence, *Pride and Berryman* [2003a] have volume averaged the local laws (1)–(4) to obtain the macroscopic "double-porosity" governing equations in the form

$$\nabla \cdot \boldsymbol{\tau}^D - \nabla P_c = -i\omega\left(\rho \mathbf{v} + \rho_f \mathbf{q}_1 + \rho_f \mathbf{q}_2\right), \tag{6}$$

$$\begin{bmatrix} \mathbf{q}_1 \\ \mathbf{q}_2 \end{bmatrix} = -\frac{1}{\eta}\begin{bmatrix} \kappa_{11} & \kappa_{12} \\ \kappa_{12} & \kappa_{22} \end{bmatrix} \cdot \begin{bmatrix} \nabla \overline{p}_{f1} - i\omega\rho_f \mathbf{v} \\ \nabla \overline{p}_{f2} - i\omega\rho_f \mathbf{v} \end{bmatrix}, \tag{7}$$

$$\begin{bmatrix} \nabla \cdot \mathbf{v} \\ \nabla \cdot \mathbf{q}_1 \\ \nabla \cdot \mathbf{q}_2 \end{bmatrix} = i\omega\begin{bmatrix} a_{11} & a_{12} & a_{13} \\ a_{12} & a_{22} & a_{23} \\ a_{13} & a_{23} & a_{33} \end{bmatrix} \cdot \begin{bmatrix} P_c \\ \overline{p}_{f1} \\ \overline{p}_{f2} \end{bmatrix} + i\omega\begin{bmatrix} 0 \\ \zeta_{\text{int}} \\ -\zeta_{\text{int}} \end{bmatrix}, \tag{8}$$

$$-i\omega\zeta_{\text{int}} = \gamma(\omega)\left(\overline{p}_{f1} - \overline{p}_{f2}\right), \tag{9}$$

$$-i\omega\boldsymbol{\tau}^D = [G(\omega) - i\omega g(\omega)]\left[\nabla \mathbf{v} + (\nabla \mathbf{v})^T - \frac{2}{3}\nabla \cdot \mathbf{v}\,\mathbf{I}\right]. \tag{10}$$

The macroscopic fields are $\mathbf{v}$, the average particle velocity of the solid grains throughout an averaging volume of the composite; $\mathbf{q}_i$, the average Darcy flux across phase i; P_c, the average total pressure in the averaging volume; $\boldsymbol{\tau}^D$, the average deviatoric stress tensor; $\overline{p}_{fi}$, the average fluid pressure within phase i; and $-i\omega\zeta_{\text{int}}$, the average rate at which fluid volume is being transferred from phase 1 into phase 2 as normalized by the total volume of the averaging region. The dimensionless increment ζ_{int} represents the "mesoscopic flow."

[18] Equation (7) is the generalized Darcy law allowing for fluid cross coupling between the phases [cf. *Pride and Berryman*, 2003b], equation (8) is the generalized compressibility law where $\nabla \cdot \mathbf{q}_i$ corresponds to fluid that has been depleted from phase i due to transfer across the external surface of an averaging volume, and equation (9) is the transport law for internal mesoscopic flow (fluid transfer between the two porous phases).

[19] The coefficients a_{ij} and γ in these equations have been modeled in detail by *Pride and Berryman* [2003a, 2003b]. Before presenting these results in sections 2.4 and 2.5, the nature of the waves implicitly contained in these laws is briefly commented upon. If plane wave solutions for $\mathbf{v}$, $\mathbf{q}_1$ and $\mathbf{q}_2$ are introduced, there is found to be a single transverse wave, and three longitudinal responses: a fast wave and two slow waves [*Berryman and Wang*, 2000]. The fast wave is the usual P wave identified on seismograms, while the two slow waves correspond to fluid pressure diffusion in phases 1 and 2. The only problem with analyzing the fast compressional wave in this manner is that the characteristic equation for the longitudinal slowness s is cubic in s^2 and therefore analytically inconvenient.

2.3. Reduction to an Effective Biot Theory

[20] The approach that we take instead is to first reduce these double-porosity laws (6)–(10) to an effective single-porosity Biot theory having complex frequency-dependent coefficients. The easiest way to do this is to assume that phase 2 is entirely embedded in phase 1 so that the average flux $\mathbf{q}_2$ into and out of the averaging volume across the external surface of phase 2 is zero. By placing $\nabla \cdot \mathbf{q}_2 = 0$

into the compressibility laws (8), the fluid pressure $\bar{p}_{f2}$ can be entirely eliminated from the theory. In this case the double-porosity laws reduce to effective single-porosity poroelasticity governed by laws of the form (3) but with effective poroelastic moduli given by

$$\frac{1}{K_D} = a_{11} - \frac{a_{13}^2}{a_{33} - \gamma/i\omega}, \tag{11}$$

$$B = \frac{-a_{12}(a_{33} - \gamma/i\omega) + a_{13}(a_{23} + \gamma/i\omega)}{(a_{22} - \gamma/i\omega)(a_{33} - \gamma/i\omega) - (a_{23} + \gamma/i\omega)^2}, \tag{12}$$

$$\frac{1}{K_U} = \frac{1}{K_D} + B\left(a_{12} - \frac{a_{13}(a_{23} + \gamma/i\omega)}{a_{33} - \gamma/i\omega}\right). \tag{13}$$

Here, $K_D(\omega)$ is the effective drained bulk modulus of the double-porosity composite, $B(\omega)$ is the effective Skempton's coefficient, and $K_U(\omega)$ is the effective undrained bulk modulus. An effective Biot-Willis constant can then be defined using $\alpha(\omega) = [1 - K_D(\omega)/K_U(\omega)]/B(\omega)$.

[21] The complex frequency-dependent "drained" modulus K_D defines the total volumetric response when the average fluid pressure throughout the host phase 1 is unchanged. Because of the fluid pressure differences between the two phases, fluid pressure equilibration ensues which results in K_D being complex and frequency-dependent. Similar interpretations hold for the undrained moduli K_U and B. An undrained response is when no fluid can escape or enter through the external surface of an averaging volume; however, there can be considerable internal exchange of fluid between the two phases resulting in the complex frequency-dependent nature of both K_U and B.

2.4. Double-Porosity a_{ij} Coefficients

[22] The constants a_{ij} are all real and correspond to the high-frequency response for which no internal fluid pressure relaxation can take place. They are given exactly as [*Pride and Berryman*, 2003a]

$$a_{11} = 1/K, \tag{14}$$

$$a_{22} = \frac{v_1\alpha_1}{K_1^d}\left(\frac{1}{B_1} - \frac{\alpha_1(1 - Q_1)}{1 - K_1^d/K_2^d}\right), \tag{15}$$

$$a_{33} = \frac{v_2\alpha_2}{K_2^d}\left(\frac{1}{B_2} - \frac{\alpha_2(1 - Q_2)}{1 - K_2^d/K_1^d}\right), \tag{16}$$

$$a_{12} = -v_1Q_1\alpha_1/K_1^d, \tag{17}$$

$$a_{13} = -v_2Q_2\alpha_2/K_2^d, \tag{18}$$

$$a_{23} = -\frac{\alpha_1\alpha_2K_1^d/K_2^d}{\left(1 - K_1^d/K_2^d\right)^2}\left(\frac{1}{K} - \frac{v_1}{K_1^d} - \frac{v_2}{K_2^d}\right), \tag{19}$$

where the Q_i are auxiliary constants given by

$$v_1Q_1 = \frac{1 - K_2^d/K}{1 - K_2^d/K_1^d} \qquad v_2Q_2 = \frac{1 - K_1^d/K}{1 - K_1^d/K_2^d}. \tag{20}$$

Here, v_1 and v_2 are the volume fractions of each phase within an averaging volume of the composite.

[23] The one constant in these a_{ij} that has not yet been determined is the overall drained modulus $K = 1/a_{11}$ of the two-phase composite (the modulus defined in the quasi-static limit where the local fluid pressure throughout the composite is everywhere unchanged). It is through K that the a_{ij} acquire their dependence on both the mesoscopic geometry and shear properties of each porous phase. Having expressions for how K depends on the properties of the two constituents is quite useful even though an exact analytical model applicable to any given double-porosity scenario may not be known.

[24] The *Hashin and Shtrikman* [1963] bounds for the overall low-frequency drained bulk modulus K and shear modulus G of the composite can be written

$$\frac{1}{K + 4G_i/3} = \frac{v_1}{K_1^d + 4G_i/3} + \frac{v_2}{K_2^d + 4G_i/3} \tag{21}$$

$$\frac{1}{G + \zeta_i} = \frac{v_1}{G_1 + \zeta_i} + \frac{v_2}{G_2 + \zeta_i}, \tag{22}$$

where ζ_i is defined

$$\zeta_i = \frac{G_i}{6}\frac{\left(9K_i^d + 8G_i\right)}{\left(K_i^d + 2G_i\right)}. \tag{23}$$

We will find it natural to define phase 2 as being more compliant than phase 1 so that $K_2^d < K_1^d$ and $G_2 < G_1$. In this case, the upper limits for K and G are obtained by taking $i = 1$ and the lower limits by taking $i = 2$. Interestingly, the upper limit is exactly realized when phase 2 is a sphere surrounded by a spherical shell of phase 1 [*Hashin*, 1962], while the lower limit is exactly realized when the differential effective medium theory of *Bruggeman* [1935] is used to model phase 2 as a collection of arbitrarily oriented penny-shaped oblate spheroids or disks [*Roscoe*, 1973].

[25] To help decide which effective medium model is most appropriate, consider the following geological situations. Any small portions of a consolidated sandstone formation that received little or no secondary mineral deposition will likely have a shape that is more dendritic than compact because mineral deposition is a transport process. Furthermore, scenarios in which thin clay lenses are engulfed by sand deposits will correspond to an embedded phase 2 geometry that is more like a penny-shaped oblate spheroid than a compact sphere. Similar comments also hold for situations in which phase 2 corresponds to macroscopic fractures or joints embedded within a stiffer sandstone host. In each of these cases, the lower *Hashin and Shtrikman* [1963] bounds are more appropriate than the upper bounds. Our modeling suggestion is simply to use the lower bounds for modeling K and G in these situations. As will be demonstrated in a numerical example, using the upper bound for K and G produces much less mesoscopic flow loss and dispersion than using the lower bound.

[26] Finally, all dependence of the a_{ij} on the fluid's bulk modulus is contained within the two Skempton's coefficients B_1 and B_2 and is thus restricted to a_{22} and a_{33}. In the quasi-static limit $\omega \to 0$ (fluid pressure everywhere uniform throughout the composite), equations (12) and (13) reduce

to the known exact results of *Berryman and Milton* [1991] once equations (14)–(19) are employed.

2.5. Double-Porosity Transport

[27] *Pride and Berryman* [2003b] obtain the internal transport coefficient γ of equation (9) as

$$\gamma(\omega) = \gamma_m \sqrt{1 - i\frac{\omega}{\omega_m}}, \tag{24}$$

where γ_m and ω_m are parameters dependent on the constituent properties and the mesoscopic geometry. To obtain useful analytical results for these two parameters, some type of approximation is required.

[28] Normally, the double-porosity model is useful (or necessary) only in situations where the two phases have strong contrasts in their physical properties. When the embedded phase 2 is much more permeable than the host phase 1, *Pride and Berryman* [2003b] obtain

$$\gamma_m = -\frac{k_1 K_1^d}{\eta L_1^2}\left(\frac{a_{12} + B_o(a_{22} + a_{33})}{R_1 - B_o/B_1}\right)[1 + O(k_1/k_2)], \tag{25}$$

where the a_{ij} are given by equations (14)–(19) and where the remaining terms B_o, L_1 and R_1 are now defined.

[29] The dimensionless quantity B_o is the static Skempton's coefficient for the composite and is given exactly by

$$B_o = -\frac{(a_{12} + a_{13})}{a_{22} + 2a_{23} + a_{33}} \tag{26}$$

regardless of the mesoscopic geometry.

[30] The length L_1 characterizes the average distance in phase 1 over which the fluid pressure gradient still exists in the final stages of equilibration and has the formal mathematical definition

$$L_1^2 = \frac{1}{V_1}\int_{\Omega_1} \Phi_1 \, dV = \frac{1}{V_1}\int_{\Omega_1} \nabla\Phi_1 \cdot \nabla\Phi_1 \, dV, \tag{27}$$

where Ω_1 is the region of an averaging volume occupied by phase 1 and having a volume measure V_1. The potential Φ_1 has units of length squared and is a solution of an elliptic boundary value problem that under conditions where the permeability ratio k_1/k_2 can be considered small, reduces to

$$\nabla^2\Phi_1 = -1 \text{ in } \Omega_1, \tag{28}$$

$$\mathbf{n} \cdot \nabla\Phi_1 = 0 \text{ on } \partial E_1, \tag{29}$$

$$\Phi_1 = 0 \text{ in } \partial\Omega_{12}. \tag{30}$$

Here, ∂E_1 is the external surface of the averaging volume coincident with phase 1, while $\partial\Omega_{12}$ is the internal interface separating phases 1 and 2. Multiplying equation (28) by Φ_1 and integrating over Ω_1, establishes that second integral of equation (27).

[31] The dimensionless quantity R_1 is the ratio of the average static confining pressure in phase 1 to the pressure applied to the external surface of a sealed sample of the composite. *Pride and Berryman* [2003a] derive this ratio to be

$$R_1 = Q_1 + \frac{\alpha_1(1 - Q_1)B_o}{1 - K_1^d/K_2^d} - \frac{v_2}{v_1}\frac{\alpha_2(1 - Q_2)B_o}{1 - K_2^d/K_1^d}, \tag{31}$$

where the Q_i are given by equation (20). Thus, once the overall drained modulus K is chosen (e.g., using the *Hashin and Shtrikman* [1963] lower bound), γ_m can now be determined from equation (25).

[32] If it is more appropriate to consider the host phase 1 as being more permeable than the embedded phase 2 ($k_2/k_1 \ll 1$), one must only exchange indices 1 and 2 throughout all of equations (25)–(31).

[33] In passing, if it is assumed that the harmonic mean is a reasonable approximation for the drained modulus of the composite (i.e., $1/K = v_1/K_1^d + v_2/K_2^d$), then $Q_i = 1$, $a_{23} = 0$, $R_1 = 1$ and all of the above expressions exactly reduce to

$$\gamma_m = \frac{v_1 k_1}{\eta L_1^2}[1 + O(k_1/k_2)]. \tag{32}$$

However, the harmonic mean for K is not always appropriate, and we consider the lower *Hashin and Shtrikman* [1963] bound as preferable for most geological situations of interest.

[34] The transition frequency ω_m corresponds to the onset of a high-frequency regime in which the fluid pressure diffusion penetration distance between the phases becomes small relative to the scale of the mesoscopic heterogeneity. It is given by *Pride and Berryman* [2003b] to be

$$\omega_m = \frac{\eta B_1 K_1^d}{k_1 \alpha_1}\left(\gamma_m \frac{V}{S}\right)^2 \left(1 + \sqrt{\frac{k_1 B_2 K_2^d \alpha_1}{k_2 B_1 K_1^d \alpha_2}}\right)^2. \tag{33}$$

The length V/S is the volume-to-surface ratio, where S is the area of $\partial\Omega_{12}$ in each volume V of composite.

2.6. Double-Porosity Modeling Choices

[35] The geometry of the phase 2 inclusion is affecting four parameters that enter the theory: the lengths L_1 and V/S as well as the drained moduli of the composite K and G. Putting in a highly complicated multiscale distribution of phase 2 (even a fractal distribution) changes the values of these four numbers but does not change the analytic structure of the above results for γ_m, ω_m, and a_{ij}.

[36] For complicated geometry, the length L_1 can only be determined numerically or inverted for from data. For idealized geometries it can be analytically estimated. For example, in a concentric sphere geometry with $k_1/k_2 \ll 1$, *Pride and Berryman* [2003b] obtain

$$L_1^2 = \frac{9}{14}R^2\left[1 - \frac{7}{6}\frac{a}{R} + O\left(a^3/R^3\right)\right],$$

where a is the radius of each sphere of phase 2 embedded within each sphere R of composite. The volume fraction v_2 of embedded spheres is $v_2 = (a/R)^3$ in this case so that R can be eliminated using $R = a/v_2^{1/3}$. In the alternative case where $k_2/k_1 \ll 1$, the length L_2 for this same concentric sphere geometry is [e.g., *Johnson*, 2001] $L_2^2 = a^2/15$.

[37] In the scenario of interest in which phase 2 is taken to be penny-shaped lenses of more compliant material mixed into a stiffer phase 1 host, the length parameter L_1 can at least be approximately estimated. Assuming that each penny-shaped inclusion has a radius a and a thickness εa where ε is the aspect ratio of the inclusion, one can estimate Φ_1 using a simple slab geometry. With the volume fraction v_2 and both a and ε treated as user-controlled parameters, one obtains that $V/S = a\varepsilon/(2v_2)$ and $L_1^2 = a^2/12$. These estimates for L_1 and V/S along with the *Hashin and Shtrikman* [1963] lower bound for K and G will be the model treated in the numerical examples that follow. Specific models for determining the properties of each porous constituent are presented in Appendix A.

[38] The coefficient $G(\omega) - i\omega g(\omega)$ governing shear generally has a nonzero "viscosity" $g(\omega)$ associated with the mesoscopic fluid transport between the compressional lobes surrounding a sheared phase 2 inclusion. Both of the frequency functions $G(\omega)$ and $-\omega g(\omega)$ are real and are Hilbert transforms of each other. The frequency dependence of $g(\omega)$ was not modeled by *Pride and Berryman* [2003b] but is presently being analyzed by these authors. Here, we continue to ignore any possible dispersion in the shear properties and take G to be a real constant given by the *Hashin and Shtrikman* [1963] lower bound.

[39] Finally, the dynamic permeability $k(\omega)$ to be used in the effective Biot theory can be modeled in several ways. The appropriate modeling choice when phase 2 is modeled as small inclusions embedded in phase 1 is the harmonic mean $1/k(\omega) = v_1/k_1(\omega) + v_2/k_2(\omega) \approx v_1/k_1(\omega)\,[1 + O(v_2 k_1/k_2)]$.

2.7. Phase Velocity and Attenuation

[40] With all of the double-porosity coefficients now defined, the compressional phase velocity and attenuation may be determined by inserting a plane wave solution into the effective single-porosity Biot equations (of the form (1)–(4)). This gives the standard complex longtitudinal slowness s of Biot theory

$$s^2 = b \mp \sqrt{b^2 - \frac{\rho\tilde{\rho} - \rho_f^2}{MH - C^2}}, \tag{34}$$

where

$$b = \frac{\rho M + \tilde{\rho} H - 2\rho_f C}{2(MH - C^2)} \tag{35}$$

is simply an auxiliary parameter and where H, C, and M are the *Biot* [1962] poroelastic moduli defined in terms of the complex frequency-dependent parameters of equations (11)–(13) as

$$H = K_U + 4G/3, \tag{36}$$

$$C = BK_U, \tag{37}$$

$$M = \frac{B^2}{1 - K_D/K_U} K_U. \tag{38}$$

The complex inertia $\tilde{\rho}$ corresponds to rewriting the relative flow resistance as an effective inertial effect

$$\tilde{\rho} = -\eta/[i\omega k(\omega)]. \tag{39}$$

Taking the minus sign in equation (34) gives an s having an imaginary part much smaller than the real part and that thus corresponds to the normal P wave. Taking the positive sign gives an s with real and imaginary parts of roughly the same amplitude and that thus corresponds to the slow P wave (a pure fluid pressure diffusion across the seismic band of frequencies). We are only interested here in the properties of the normal P wave.

[41] The P wave phase velocity v_p and the attenuation measure Q_p^{-1} are related to the complex slowness s as

$$v_p = 1/\mathrm{Re}\{s\} \tag{40}$$

$$Q_p^{-1} = \mathrm{Im}\{s^2\}/\mathrm{Re}\{s^2\}. \tag{41}$$

2.8. Numerical Examples

[42] In Figure 1, we give an example of Q_p^{-1} and v_p as determined using the double-porosity theory. The example models a consolidated sandstone phase 1 host that contains thin lenses (squashed/oblate spheroids) of an uncemented granular phase 2 material. The drained properties of phase 2 are determined using the modified Walton theory given in Appendix A. In this way, the moduli K_2^d and G_2 are functions of the background effective stress level P_e. The host phase 1 is modeled using $\phi_1 = 0.20$ and $c = 2$ in the model given in Appendix A. All mineral moduli are taken to be that of quartz $K_s = 38$ GPa and $G_s = 44$ GPa and the permeability of the host phase is $k_1 = 10$ mdarcy. The drained properties of the composite were modeled using the *Hashin and Shtrikman* [1963] lower bounds given in equations (21) and (22). The penny-shaped inclusion of phase 2 have the following geometric properties: $a = 3$ cm, $\varepsilon = 10^{-2}$, $v_2 = 3\%$, $L_1 = 8.6$ mm, and $V/S = 5$ mm. The specific shape of the attenuation curve is highly sensitive to whether L_1 is greater than or less than V/S. The invariant peak near 10^6 Hz is that due to the Biot loss (fluid equilibration at the scale of the seismic wavelength), while the broad principal peak that changes with the effective pressure P_e is that due to mesoscopic-scale equilibration. All dependence on P_e in this example comes from how K_2^d and G_2 vary with P_e.

[43] The level of attenuation in the double-porosity theory is controlled by the factors that allow phase 2 to develop a different fluid pressure response as compared to phase 1. In Figure 2, this is demonstrated by comparing phase 2 modeled as spheres to phase 2 modeled as penny-shaped lenses. Both examples have identically the same volume fractions of phase 2 as well as phase 1 and 2 material properties. The difference is that in the sphere model, the *Hashin and Shtrikman* [1963] upper bound is used for K and G while the lower bound is used in the penny-shaped lens model. A compliant sphere of phase 2 is protected from an applied compression by the rigidity of the phase 1 host that surrounds it. Accordingly, not much fluid pressure difference is created between the two phases and so there is only a small amount of mesoscopic loss.

[44] In modeling the penny-shaped inclusions in Figure 2, we have used the parameter values $a = 3$ cm (inclusion radius) and $\varepsilon = 10^{-1}$ to obtain $V/S = 5$ cm and $L_1 = 0.9$ cm. In this case, $V/S > L_1$ which has changed considerably the look of the attenuation curve as compared to Figure 1 where

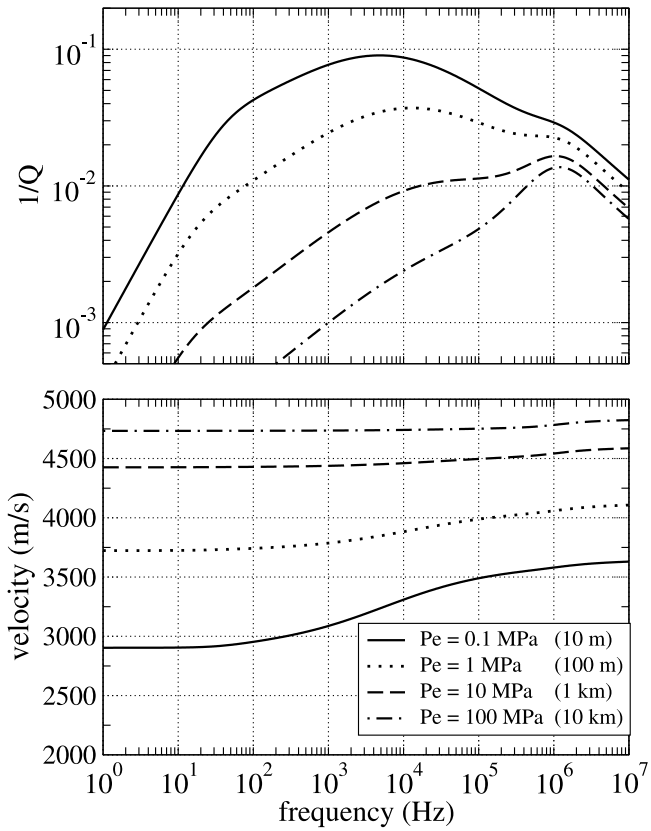

Figure 1. Attenuation and phase velocity of compressional waves in the double-porosity model of *Pride and Berryman* [2003a]. The thin lenses of phase 2 have frame moduli (K_2^d and G_2) modeled using the modified *Walton* [1987] theory given in Appendix A in which both K_2^d and G_2 vary strongly with the background effective pressure P_e (or overburden thickness). These lenses of porous continuum 2 are embedded into a phase 1 continuum modeled as a consolidated sandstone.

$V/S < L_1$. What is happening can be seen in the effective moduli of equations (11)–(13). The principal relaxation in the effective moduli occurs whenever $\omega = \gamma/a_{ij}$. However, there is also a relaxation in $\gamma(\omega)$ when $\omega = \omega_m$. For situations where $V/S \gg L_1$, the effective moduli relax at a frequency much less than ω_m (with $\gamma(\omega) = \gamma_m$). This is the case in Figure 2. When $V/S < L_1$, the relaxation in $\gamma(\omega)$ can begin prior to the principal relaxation as is seen in Figure 1.

[45] Finally, in Figure 3, we compare the double-porosity model to the data of *Sams et al.* [1997], who used different seismic measurements (VSP, cross-well, sonic log, and ultrasonic lab) to determine Q^{-1} and P wave velocity over a wide band of frequencies at their test site in England. The variance of the measurements falling within each rectangular box are due to the various rock layers present at this site. Data collection was between four wells that are a few hundred meters deep. The geology at the site is a sequence of layered limestones, sandstones, siltstones and mudstones. We model phase 2 as unconsolidated penny-shaped inclusions in which $a = 5$ cm (inclusion radius), $\varepsilon = 6 \times 10^{-3}$, $v_2 = 1.2\%$, $k_1 = 80$ mdarcy, $V/S = 1.25$ cm, and $L_1 = 1.45$ cm. The phase 1 host is taken to be a well-consolidated sandstone ($\phi_1 = 0.20$ and $c = 1$).

2.9. Discussion

[46] The overall magnitude of attenuation in the double-porosity model is dominantly controlled both by the contrast of compressibilities between the two porous phases and the assumed shape of the embedded phase. Certain assumed shapes, such as spherical inclusions, allow the rigidity of the host phase to protect even a soft inclusion from being compressed much and this results in minimal mesoscopic loss for such a geometry. Less compact and more elongated or even dendritic mesoscopic geometries are what potentially allow the mesoscopic loss to be important. However, even in the presence of such structure, a strong contrast in the drained properties of the two phases is also required in order to generate a significant mesoscopic fluid pressure gradient and mesoscopic loss. A contrast in permeability alone would generate no such mesoscopic-scale fluid pressure gradients.

[47] The relaxation frequency at which the mesoscopic loss per cycle is maximum is proportional to $k_1/(\eta L_1^2)$. Far below this relaxation frequency, Q^{-1} always increases linearly with frequency as $f\eta/k_1$. Thus the permeability information in the double-porosity attenuation is principally in the frequency dependence of Q^{-1}, not in the overall magnitude of Q^{-1}, and involves principally the permeability

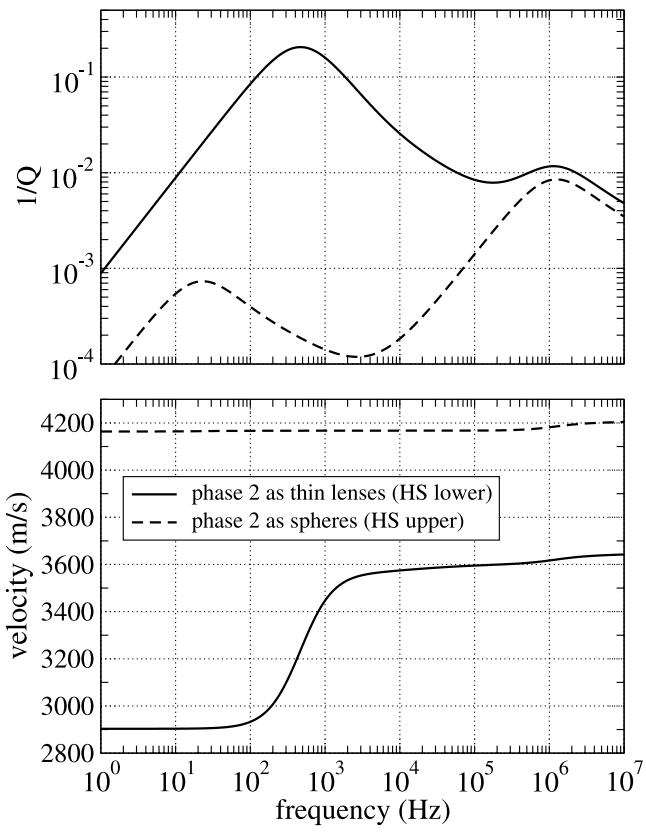

Figure 2. A comparison of modeling the embedded phase 2 as either penny-shaped lenses or spheres. All curves have identical phase 1 and phase 2 material properties and identical phase 2 volume fractions $v_2 = 2\%$. The only difference is the assumed shape of the phase 2 inclusion which has a strong influence on the overall drained bulk modulus of the composite (the *Hashin and Shtrikman* [1963] upper bound holds in the case of spheres, while the lower bound holds in the case of penny-shaped lenses).

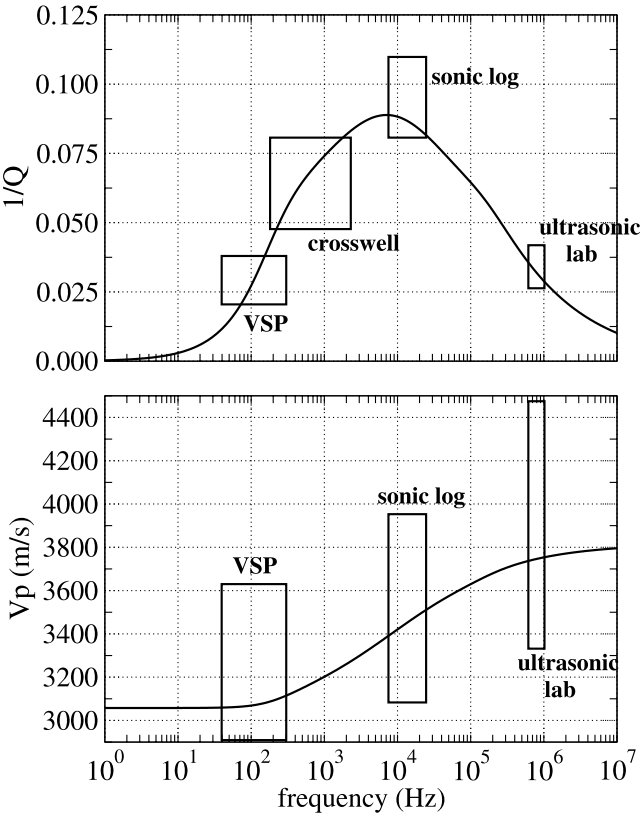

Figure 3. Attenuation and dispersion predicted by the double-porosity model of *Pride and Berryman* [2003a] (the solid curves) as compared to the data of *Sams et al.* [1997] (rectangular boxes). The number of Q^{-1} estimates determined by *Sams et al.* [1997] falling within each rectangular box are 40 VSP, 69 cross-well, 854 sonic log, and 46 ultrasonic core measurements. A similar number of velocity measurements were made. These various measurements come from different depth ranges at their test site.

k_1 of the host phase, not the overall permeability of the composite (see *Berryman* [1988] for a related discussion). If phase 2 is well modeled as being small penny-shaped inclusions embedded in phase 1, then k_1 is controlling the overall permeability. If phase 2 corresponds to throughgoing connected joints, then although $Q^{-1}(\omega)$ contains information about k_1, it does not contain information about the overall permeability which is being dominated by k_2 in this case (i.e., k_2 has no significant influence on the mesoscopic loss process).

[48] In the case of throughgoing joints, the equilibration at the scale of the wavelength (the Biot loss) has a chance of being shifted to lower frequencies. The only way to determine the proper attenuation curve in this case is to solve the cubic characteristic equation for s^2 (the characteristic equation is obtained by inserting a plane wave solution into the complete double-porosity equations (6)–(10), as discussed earlier).

3. Patchy Saturation Model

[49] Another important source of mesoscopic-scale heterogeneity having an important influence on seismic properties is patchy fluid saturation [e.g., *Knight et al.*, 1998]. All natural hydrological processes by which one fluid nonmiscibly invades a region initially occupied by another result in a patchy distribution of the two fluids. The patch sizes are distributed across the entire range of mesoscopic length scales and for many invasion scenarios are expected to be fractal. As a compressional wave squeezes such a material, the patches occupied by the less compressible fluid will respond with a greater fluid pressure change than the patches occupied by the more compressible fluid. The two fluids will then equilibrate by the same type of mesoscopic flow already modeled in the double-porosity model.

[50] An analysis almost identical to that of *Pride and Berryman* [2003a, 2003b] can be carried out that leads to the same effective poroelastic moduli given by equations (11)–(13) but with different definitions of the a_{ij} constants and internal transport coefficient $\gamma(\omega)$. In the model, a single uniform porous frame is saturated by mesoscopic-scale patches of fluid 1 and fluid 2. We define porous phase 1 to be those regions (patches) occupied by the less mobile fluid and phase 2 the patches saturated by the more mobile fluid, i.e., by definition, $\eta_1 > \eta_2$. This most often (but not necessarily) corresponds to $K_{f1} > K_{f2}$ and therefore to $B_1 > B_2$.

[51] *Johnson* [2001] has treated this model using a different coarse-graining argument while starting from the same local physics (however, he assumes the porous material is a Gassmann monomineral material). Our final undrained bulk modulus is identical to the result of *Johnson* [2001] in the limits of high and low frequency and differs only negligibly in the transition range of frequencies where the flow in either model is not explicitly treated.

3.1. Patchy Saturation a_{ij} Coefficients

[52] To obtain the a_{ij} for the patchy saturation model, we note that by model assumption, each patch has the same α and K. The poroelastic differences between patches is entirely due to B_1 being different than B_2. Upon averaging equation (3) and using $\nabla \cdot \mathbf{v} = \nabla \cdot (v_1 \dot{\bar{\mathbf{u}}}_1) + \nabla \cdot (v_2 \dot{\bar{\mathbf{u}}}_2)$, where an overline again denotes a volume average over the appropriate phase, and using the fact that the a_{ij} are defined in the extreme high-frequency limit where the fluids have no time to traverse the internal interface $\partial\Omega_{12}$ (i.e., the a_{ij} are defined under the condition that $\dot{\zeta}_{\text{int}} = 0$), one has

$$\nabla \cdot \mathbf{v} = -\frac{v_1}{K}\dot{\bar{p}}_{c1} - \frac{v_2}{K}\dot{\bar{p}}_{c2} + \frac{v_1\alpha}{K}\dot{\bar{p}}_{f1} + \frac{v_2\alpha}{K}\dot{\bar{p}}_{f2}, \tag{42}$$

$$\nabla \cdot \mathbf{q}_1 = \frac{v_1\alpha}{K}\dot{\bar{p}}_{c1} - \frac{v_1\alpha}{KB_1}\dot{\bar{p}}_{f1}, \tag{43}$$

$$\nabla \cdot \mathbf{q}_2 = \frac{v_2\alpha}{K}\dot{\bar{p}}_{c2} - \frac{v_2\alpha}{KB_2}\dot{\bar{p}}_{f2}. \tag{44}$$

The average confining pressures $\bar{p}_{ci}$ in each phase are not a priori known; however, they are necessarily linear functions of the three independent applied pressures of the theory $P_c (= v_1\bar{p}_{c1} + v_2\bar{p}_{c2})$, $\bar{p}_{f1}$, and $\bar{p}_{f2}$. It is straightforward to demonstrate that if and only if the average confining pressures take the form

$$v_1\dot{\bar{p}}_{c1} = v_1\dot{P}_c + \beta\dot{\bar{p}}_{f1} - \beta\dot{\bar{p}}_{f2} \tag{45}$$

$$v_2\dot{\bar{p}}_{c2} = v_2\dot{P}_c - \beta\dot{\bar{p}}_{f1} + \beta\dot{\bar{p}}_{f2}, \tag{46}$$

will equations (42)–(44) produce a_{ij} that satisfy the thermodynamic symmetry requirement of $a_{ij} = a_{ji}$ (i.e., these a_{ij} constants are all second derivatives of a strain energy function as demonstrated by *Pride and Berryman* [2003a]). Upon placing equations (45) and (46) into equations (42)–(44), we then have

$$a_{11} = 1/K, \tag{47}$$

$$a_{22} = (-\beta + v_1/B_1)\alpha/K, \tag{48}$$

$$a_{33} = (-\beta + v_2/B_2)\alpha/K, \tag{49}$$

$$a_{12} = -v_1\alpha/K, \tag{50}$$

$$a_{13} = -v_2\alpha/K, \tag{51}$$

$$a_{23} = \beta\alpha/K, \tag{52}$$

where β is the single constant remaining to be determined.

[53] To obtain β, we note that in the high-frequency limit, each local patch of phase i is undrained and thus characterized by an undrained bulk modulus $K_i^u = K/(1 - \alpha B_i)$ and a shear modulus G that is the same for all patches. In this limit, the usual laws of elasticity (as opposed to those of poroelasticity) govern the response of the composite. Note that, even if the rock frame is spatially uniform, an exception to uniform G can, in principle, occur if cracks are uniformly present. In this case, it is known [see *Berryman et al.*, 2002] that the shear modulus in the regions containing dry cracks can be somewhat different from the shear modulus in the regions containing wet cracks. In reality, however, all cracks tend to be water wet in partially saturated rocks and it is a physically reasonable approximation to assume that G is the same for each phase even when cracks are present.

[54] Under these precise conditions (elasticity of an isotropic composite having uniform G and all heterogeneity confined to the bulk modulus which in the present case corresponds to K_i^u), we follow *Johnson* [2001] by invoking the theorem of *Hill* [1963], which states that the overall undrained-unrelaxed modulus of the composite K_H is given exactly by

$$\frac{1}{K_H + 4G/3} = \frac{v_1}{K_1^u + 4G/3} + \frac{v_2}{K_2^u + 4G/3}. \tag{53}$$

In terms of the a_{ij}, this same undrained-unrelaxed Hill modulus is given by

$$\frac{1}{K_H} = a_{11} + a_{12}\left(\frac{\delta p_{f1}}{\delta P_c}\right)_U + a_{13}\left(\frac{\delta p_{f2}}{\delta P_c}\right)_U, \tag{54}$$

where upon using $\nabla \cdot \mathbf{q}_i = 0$ and $\dot{\zeta}_{\text{int}} = 0$ in equation (8) and then using (47)–(52), the undrained-unrelaxed pressure ratios are

$$\left(\frac{\delta p_{f1}}{\delta P_c}\right)_U = \frac{\beta - v_1 v_2/B_2}{\beta(v_1/B_1 + v_2/B_2) - v_1 v_2/(B_1 B_2)} \tag{55}$$

$$\left(\frac{\delta p_{f2}}{\delta P_c}\right)_U = \frac{\beta - v_1 v_2/B_1}{\beta(v_1/B_1 + v_2/B_2) - v_1 v_2/(B_1 B_2)}. \tag{56}$$

Thus, after some algebra, equation (54) yields the exact result

$$\beta = v_1 v_2 \left(\frac{v_1}{B_2} + \frac{v_2}{B_1}\right)\left[\frac{\alpha - (1 - K/K_H)/(v_1 B_1 + v_2 B_2)}{\alpha - (1 - K/K_H)(v_1/B_1 + v_2/B_2)}\right] \tag{57}$$

with K_H given by equation (53). All the a_{ij} are now expressed in terms of known information.

3.2. Patchy Saturation Transport

[55] Next, we must address the internal fluid pressure equilibration between the two phases with the goal of obtaining the internal transfer coefficient γ of equation (9). The mathematical definition of the rate of internal fluid transfer is

$$\dot{\zeta}_{\text{int}} = \frac{1}{V}\int_{\partial\Omega_{12}} \mathbf{n} \cdot \mathbf{Q}_1 \, dS, \tag{58}$$

where V is the volume occupied by the composite. A possible concern in the patchy saturation analysis is whether capillary effects at the local interface $\partial\Omega_{12}$ separating the two phases need to be considered.

3.2.1. Capillary Effects

[56] At the pore scale, the interface separating one fluid patch from the next is a series of meniscii. Roughness on the grain surfaces keeps the contact lines of these meniscii pinned to the grain surfaces. *Pride and Flekkoy* [1999] argue that the contact lines of an air-water meniscus will remain pinned for fluid pressure changes less than roughly 10^4 Pa, which corresponds to the pressure range induced by linear seismic waves. So as a wave passes, the meniscii will bulge and change shape but will not migrate away.

[57] For the fluid pressure equilibration problem, one porous continuum boundary condition is that all fluid volume that locally enters the interface $\partial\Omega_{12}$ from one side, must exit the other side so that $\mathbf{n} \cdot \mathbf{Q}_1 = \mathbf{n} \cdot \mathbf{Q}_2 (= \mathbf{n} \cdot \mathbf{Q})$. Another boundary condition is that the rate at which the fluid pressure difference across the interface is changing is equal to the surface tension multiplied by the rate at which the mean curvature of the meniscii is changing. At the level of the porous continuum, this boundary condition may be written [cf. *Nagy and Blaho*, 1994; *Nagy and Nayfeh*, 1995; *Tserkovnyak and Johnson*, 2003]

$$\frac{\partial p_{f1}}{\partial t} - \frac{\partial p_{f2}}{\partial t} = W \mathbf{n} \cdot \mathbf{Q} \quad \text{on} \quad \partial\Omega_{12} \tag{59}$$

where W is called the membrane stiffness. For cylindrical tube models of the pore space, one has [e.g., *Nagy and Blaho*, 1994] $W = \sigma/k$ (where σ is the surface tension and k is the permeability) showing that surface tension effects become more important in tighter rocks. As $W \to 0$, the surface tension provides no resistance to the equilibration while as $W \to \infty$, the interface becomes effectively sealed to flow at all frequencies.

[58] *Tserkovnyak and Johnson* [2003] have performed a complete analysis of the undrained response problem in the presence of finite W culminating in an analytic expression for the complex frequency-dependent undrained bulk modulus. The dominant effect of finite W is to increase the low-frequency undrained modulus while leaving the

high-frequency limit unchanged since this limit already corresponds to no fluid equilibration. As $W \to \infty$, there is no dispersion in the bulk modulus since the fluid in each patch remains in the patch at all frequencies.

[59] Here, we only seek to define the precise conditions for which the surface tension (or capillary) effects may be neglected in the static limit where such effects are the most important. To do so, we follow *Tserkovnyak and Johnson* [2003] and integrate equation (59) over $\partial\Omega_{12}$ and over time. Equation (58) may be employed along with the fact that $p_{fi}(\mathbf{r}) = \bar{p}_{fi}$ are spatial constants to give

$$\bar{p}_{f1} - \bar{p}_{f2} = \frac{V}{S} W \zeta_{\text{int}}, \tag{60}$$

where S is the amount of fluid interface within a sample of volume V. If this expression for ζ_{int} is used in equation (8) along with sealed sample conditions ($\nabla \cdot \mathbf{q}_1 = \nabla \cdot \mathbf{q}_2 = 0$), one can solve for both $\bar{p}_{f1}$ and $\bar{p}_{f2}$ and take their difference. The a_{ij} constants of section 3.1 are unaffected by W since they are defined in the high-frequency limit of no fluid equilibration. In this manner, one obtains that the key dimensionless number $\mathcal{C}$ controlling whether $\bar{p}_{f1} \neq \bar{p}_{f2}$ at low frequencies and therefore controlling the importance of capillary effects in the elastic response is (assuming $B_1 > B_2$)

$$\mathcal{C} = W \frac{V}{S} \frac{\alpha(\beta - v_1 v_2 / B_2)}{K}. \tag{61}$$

When $\mathcal{C} \ll 1$, surface tension plays absolutely no role in the effective moduli. When $\mathcal{C} \gg 1$, there is no acoustic dispersion or attenuation because the surface tension keeps the fluid patches from equilibrating. If $B_2 > B_1$, one should replace B_2 with B_1 in the definition of $\mathcal{C}$.

[60] One way to be in the limit where surface tension is negligible is to have the fluid bulk moduli in each patch very similar. In this case, $\beta \to v_1 v_2 / B_2$ and $\mathcal{C} \to 0$. However, in this case there is not much attenuation and dispersion since there is not much mesoscopic flow induced by the wave.

[61] Using $W = \sigma / k$ for making estimates, one finds that for surface tension to be negligible the inequality

$$\frac{\sigma V / S}{kK} < 1 \tag{62}$$

must hold. Using the common sandstone values of k = 100 mdarcy, K = 10 GPa, and $\sigma \approx 10^{-2}$ Pa m (order of magnitude appropriate for water/air and water/oil meniscii), one obtains that V/S should be smaller than roughly 10^{-1} m for surface tension effects to be negligible. In what follows, we only treat the regime $\mathcal{C} \ll 1$ which is the regime also studied by *Johnson* [2001].

3.2.2. Mesoscopic Flow Equations

[62] To obtain the transport law $-i\omega\zeta_{\text{int}} = \gamma(\omega)(\bar{p}_{f1} - \bar{p}_{f2})$, the mesoscopic flow is analyzed in the limits of low and high frequencies. These limits are then connected using a frequency function that respects causality constraints. The linear fluid response inside the patchy composite due to a seismic wave can always be resolved into two portions: (1) a vectorial response due to macroscopic fluid pressure gradients across an averaging volume that generate a macroscopic Darcy flux $\mathbf{q}_i$ across each phase and that corresponds to the macroscopic conditions $\bar{p}_{fi} = 0$ and $\nabla \bar{p}_{fi} \neq 0$; and (2) a scalar response associated with internal fluid transfer and that corresponds to the macroscopic conditions $\bar{p}_{fi} \neq 0$ and $\nabla \bar{p}_{fi} = 0$. The macroscopic isotropy of the composite guarantees that there is no cross coupling between the vectorial transport $\mathbf{q}_i$ and the scalar transport ζ_{int} within each sample ("Curie's principle" which is, in fact, a theorem [cf. *deGroot and Mazur*, 1984]).

[63] The mesoscopic flow problem that defines $\dot{\zeta}_{\text{int}}$ is the internal equilibration of fluid pressure between the patches when a confining pressure ΔP has been applied to a sealed sample of the composite. Having the external surface sealed is equivalent to the required macroscopic constraint that $\nabla \bar{p}_{fi} = 0$. Upon taking the divergence of equation (2) and using equation (3), the diffusion problem controlling the mesoscopic flow becomes

$$\frac{k}{\eta_i} \nabla^2 p_{fi} + i\omega \frac{\alpha}{KB_i} p_{fi} = i\omega \frac{\alpha}{K} p_{ci} \quad \text{in} \quad \Omega_i, \tag{63}$$

$$\left[p_{fi}\right] = 0 \quad \left[\mathbf{n} \cdot \nabla p_{fi}\right] = 0 \quad \text{on} \quad \partial\Omega_{12}, \tag{64}$$

$$\mathbf{n} \cdot \nabla p_{fi} = 0 \quad \text{on} \quad \partial E_i, \tag{65}$$

where Ω_i is the region that each phase occupies within the averaging volume, ∂E_i is that portion of the external surface of the averaging volume that is in contact with phase i, and the brackets in equation (64) again denote jumps across the interface. One also needs to insert equations (3) and (4) into equation (1) to obtain a second-order partial differential equation for the displacements $\mathbf{u}_i$. In general, the local confining pressures p_{ci} are determined using

$$p_{ci} = -K \nabla \cdot \mathbf{u}_i + \alpha p_{fi} \tag{66}$$

once the displacements $\mathbf{u}_i$ are known.

3.2.3. Low-Frequency Limit of $\gamma(\omega)$

[64] As $\omega \to 0$, we can represent the local fields as perturbation expansions in the small parameter $-i\omega$ [e.g., *Johnson*, 2001]

$$p_{fi} = p_{fi}^{(0)} - i\omega p_{fi}^{(1)} + O(\omega^2) \tag{67}$$

$$p_{ci} = p_{ci}^{(0)} - i\omega p_{ci}^{(1)} + O(\omega^2), \tag{68}$$

and equivalently for $\mathbf{u}_i$. The zeroth-order response corresponds to uniform fluid pressure in the pores and is therefore given by $p_{c1}^{(0)} = p_{c2}^{(0)} = \Delta P$ and

$$\frac{\bar{p}_{fi}^{(0)}}{\Delta P} = B_o = -\frac{a_{12} + a_{13}}{a_{22} + 2a_{23} + a_{33}} = \frac{1}{v_1/B_1 + v_2/B_2}, \tag{69}$$

where the patchy saturation a_{ij} have been employed. The fact that the quasi-static Skempton's coefficient in the patchy saturation model is exactly the harmonic average of the constituents B_i is equivalent to saying that at low frequencies, the fluid bulk modulus is given by $1/K_f = v_1/K_{f1} + v_2/K_{f2}$. The quasi-static response is thus completely

independent of the spatial geometry of the fluid patches; it depends only on the volume fractions occupied by the patches.

[65] The leading order correction to uniform fluid pressure is then controlled by the boundary value problem

$$\frac{Kk}{\alpha\eta_1}\nabla^2 p_{f2}^{(1)} = \frac{\eta_2}{\eta_1}\left(1-\frac{B_o}{B_2}\right)\Delta P \quad \text{in} \quad \Omega_2, \tag{70}$$

$$\frac{Kk}{\alpha\eta_1}\nabla^2 p_{f1}^{(1)} = \left(1-\frac{B_o}{B_1}\right)\Delta P \quad \text{in} \quad \Omega_1, \tag{71}$$

$$p_{f1}^{(1)} = p_{f2}^{(1)} \quad \text{on} \quad \partial\Omega_{12}, \tag{72}$$

$$\mathbf{n}\cdot\nabla p_{f2}^{(1)} = \frac{\eta_2}{\eta_1}\mathbf{n}\cdot\nabla p_{f1}^{(1)} \quad \text{on} \quad \partial\Omega_{12}, \tag{73}$$

$$\mathbf{n}\cdot\nabla p_{fi}^{(1)} = 0 \quad \text{on} \quad \partial E_i. \tag{74}$$

It is now assumed that for patchy saturation cases of interest (air/water or water/oil), the ratio η_2/η_1 can be considered small. To leading order in η_2/η_1, equations (70), (73), and (74) require that $p_{f2}^{(1)}(\mathbf{r}) = \bar{p}_{f2}^{(1)}$ (a spatial constant). The fluid pressure in phase 1 is now rewritten as

$$p_{f1}^{(1)}(\mathbf{r}) = \bar{p}_{f2}^{(1)} - \frac{\eta_1\alpha}{kK}\left(1-\frac{B_o}{B_1}\right)\Delta P\Phi_1(\mathbf{r}), \tag{75}$$

where, from equations (71), (72) and (74) and to leading order in η_2/η_1, the potential Φ_1 is the solution of the same elliptic boundary value problem (28)–(30) given earlier.

[66] Upon averaging (75) over all of Ω_1, the leading order in $-i\omega$ difference in the average fluid pressures can be written

$$\frac{\bar{p}_{f1}-\bar{p}_{f2}}{\Delta P} = -i\omega\left(\frac{\bar{p}_{f1}^{(1)}-\bar{p}_{f2}^{(1)}}{\Delta P}\right) = i\omega\frac{\eta_1\alpha}{kK}\left(1-\frac{B_o}{B_1}\right)L_1^2, \tag{76}$$

where L_1 is again the length defined by equation (27).

[67] To connect this fluid pressure difference to the increment $\dot{\zeta}_{\text{int}}$, we use the divergence theorem and the no-flow boundary condition on ∂E_i to write equation (58) as

$$-i\omega\zeta_{\text{int}} = \frac{i\omega}{V}\frac{k}{\eta}\int_{\partial\Omega_{12}}\mathbf{n}\cdot\nabla p_{f1}^{(1)}\,dS = i\omega v_1\frac{\alpha}{K}\left(1-\frac{B_o}{B_1}\right)\Delta P. \tag{77}$$

Replacing ΔP with $\bar{p}_{f1}-\bar{p}_{f2}$ using equation (76) then gives the desired law $-i\omega\zeta_{int} = \gamma_p\,(\bar{p}_{f1}-\bar{p}_{f2})$ with

$$\gamma_p = \frac{v_1 k}{\eta_1 L_1^2}\left[1+O\left(\frac{\eta_2}{\eta_1}\right)\right] \tag{78}$$

being the low-frequency limit of interest.

3.2.4. High-Frequency Limit of γ(ω)

[68] It has already been commented that in the extreme high-frequency limit where each patch behaves as if it were sealed to flow ($\dot{\zeta}_{\text{int}} = 0$), the theory of *Hill* [1963] applies (so long as all cracks are water wet). Hill demonstrated, among other things, that when each isotropic patch has the same shear modulus, the volumetric deformation within each patch is a spatial constant. The fluid pressure response in this limit p_{fi}^{∞} is thus a uniform spatial constant throughout each phase except in a vanishingly small neighborhood of the interface $\partial\Omega_{12}$ where equilibration is attempting to take place. The small amount of fluid pressure penetration that is occurring across $\partial\Omega_{12}$ can be locally modeled as a one-dimensional process normal to the interface.

[69] Using the coordinate x to measure linear distance normal to the interface (and into phase 1), one has that equation (63) is satisfied by [*Johnson*, 2001]

$$p_{f1} = p_{f1}^{\infty} + C_1 e^{i\sqrt{i\omega/D_1}\,x} \tag{79}$$

$$p_{f2} = p_{f2}^{\infty} + C_2 e^{-i\sqrt{i\omega/D_1}\,x}, \tag{80}$$

where the diffusivities are defined $D_i = kKB_i/(\eta_i\alpha)$. The constants C_i are found from the continuity conditions (64) to be

$$C_1 = \frac{-1}{1+\sqrt{\eta_2 B_2/(\eta_1 B_1)}}\left(p_{f1}^{\infty}-p_{f2}^{\infty}\right) \tag{81}$$

$$C_2 = \frac{\sqrt{\eta_2 B_2/(\eta_1 B_1)}}{1+\sqrt{\eta_2 B_2/(\eta_1 B_1)}}\left(p_{f1}^{\infty}-p_{f2}^{\infty}\right). \tag{82}$$

Although not actually needed here, we have that $p_{fi}^{\infty} = B_i p_{ci}$, where the uniform confining pressure of each patch is given by equations (45) and (46), so that the fluid pressure difference between the phases goes as

$$\frac{p_{f1}^{\infty}-p_{f2}^{\infty}}{\Delta P} = \frac{B_1-B_2}{1-\beta(B_1/\nu_1+B_2/\nu_2)}. \tag{83}$$

Equation (83) is exactly the difference between equations (55) and (56). Because the penetration distance $\sqrt{D_i/\omega}$ vanishes at high frequencies, we may state that to leading order in the high-frequency limit, $\bar{p}_{f1}-\bar{p}_{f2} = p_{f1}^{\infty}-p_{f2}^{\infty}$.

[70] To obtain the high-frequency limit of the transport coefficient $\gamma(\omega)$, we use the definition (58) of the internal transport (note that $-\mathbf{n}\cdot\nabla p_{f1} = \partial p_{f1}/\partial x$)

$$-i\omega\zeta_{\text{int}} = \frac{1}{V}\frac{k}{\eta_1}\int_{\partial\Omega_{12}}\frac{\partial p_{f1}}{\partial x}\,dS \tag{84}$$

along with equations (79) and (81). The result is

$$\gamma(\omega) \sim i^{3/2}\sqrt{\omega}\frac{S}{V}\left(\frac{\sqrt{k\alpha/(\eta_1 B_1 K)}}{1+\sqrt{\eta_2 B_2/(\eta_1 B_1)}}\right) \tag{85}$$

as $\omega \to \infty$. Here, S is again the area of $\partial\Omega_{12}$ contained within a volume V of the patchy composite.

3.2.5. Full Model for γ(ω)

[71] The high- and low-frequency limits of γ are then connected by a simple frequency function to obtain the final model

$$\gamma(\omega) = \gamma_p\sqrt{1-i\omega/\omega_p}, \tag{86}$$

where the transition frequency ω_p is defined

$$\omega_p = \frac{B_1 K}{\eta_1\alpha}\frac{k(v_1 V/S)^2}{L_1^4}\left(1+\sqrt{\frac{\eta_2 B_2}{\eta_1 B_1}}\right)^2, \tag{87}$$

and where $\gamma_p = v_1 k/(\eta_1 L_1^2)$. Equation (86) has a single singularity (a branch point) at $\omega = -i\omega_p$. Causality requires that with an $e^{-i\omega t}$ time dependence, all singularities and

zeroes of a transport coefficient like $\gamma(\omega)$ must reside in the lower half complex ω plane. Equation (86) satisfies this physically important constraint.

3.3. Patchy Saturation Modeling Choices

[72] To use the patchy saturation model, appropriate values for the two geometric terms L_1 and V/S must be specified. Immiscible fluid distributions in the earth have very complicated geometries since they arise from slow flow that often produces fractal patch distributions. In particular, analytical solutions of the boundary value problem (28)–(30) that defines L_1 for such real Earth situations are impossible. Recall that L_1 is a characteristic length of phase 1 (the phase having the smaller fluid mobility k/η) that defines the distance over which the fluid pressure gradient is defined during the final stages of equilibration. For complicated geometries it may either be numerically determined, treated as a target parameter for a full waveform inversion of seismic data, or simply estimated qualitatively. In the numerical examples that follow, we will assume (for convenience) that the individual patches correspond to disconnected spheres for which simple analytical results are available for L_1 and V/S.

[73] If we consider phase 2 (porous continuum saturated by the less viscous fluid) to be in the form of spheres of radius a embedded within each radius R sphere of the two-phase composite, then $v_2 = (a/R)^3$, $V/S = av_2/3$, and $L_1^2 = 9v_2^{-2/3}a^2/14[1 - 7v_2^{1/3}/6]$. This model is particularly appropriate when $v_2 \ll v_1$. Since the fluid 2 patches are disconnected, the definitions (11)–(13) of the effective poroelastic moduli again hold. Furthermore, fluid 2 may be taken to be immobile relative to the framework of grains in the wavelength-scale Biot equilibration so that the inertial properties of equations (34) and (35) are identified as $\rho_f = \rho_{f1}$, $\rho = (1 - \phi)\rho_s + \phi(v_1\rho_{f1} + v_2\rho_{f2})$ and $\tilde{\rho} = -\eta_1/(i\omega k)$.

[74] In situations where it is more appropriate to treat fluid 1 (the more viscous fluid) as occupying disconnected patches (e.g., when $v_1 \ll v_2$), the effective poroelastic moduli are defined by interchanging 2 and 3 in the subscripts of equations (11)–(13). Again assuming the phase 1 patches to be spheres of radius a embedded within each radius R sphere of the two-phase composite, we have that $v_1 = (a/R)^3$ and $V/S = av_1/3$. The elliptic boundary value problem (28)–(30) can be solved in this case to give $L_1^2 = a^2/15$. Furthermore, the effective inertial coefficients in the Biot theory are defined $\rho_f = \rho_{f2}$, $\rho = (1 - \phi)\,\rho_s + \phi(v_1\rho_{f1} + v_2\rho_{f2})$, and $\tilde{\rho} = -\eta_2/(i\omega k)$.

[75] In situations where both phases form continuous paths across each averaging volume, it is best to determine the attenuation and phase velocity by seeking the plane longtitudinal wave solution of nonreduced "double-porosity" governing equations of the form (6)–(10). However, this approach is not pursued here. We conclude by noting that, if the embedded fluid is fractally distributed, the lengths L_1 will remain finite while $(V/S)/L_1 \rightarrow 0$ as the fractal surface area S becomes large (however, V/S never reaches zero because the fractality has a small-scale cutoff fixed by the grain size of the material).

3.4. Numerical Examples

[76] In Figure 4 we compare the *Johnson* [2001] prediction of K_U to our own for a consolidated sandstone (frame properties as determined in Appendix A with $k = 100$ mdarcy, $c = 10$, $\phi = 0.20$) in which phase 1 is saturated with water and phase 2 is taken to be spherical regions saturated with air. The two estimates have identical asymptotic dependence in both the limits of high and low frequencies. In the crossover range, the physics is not precisely modeled in either approach. However, even in the crossover range, the differences in the two models is slight.

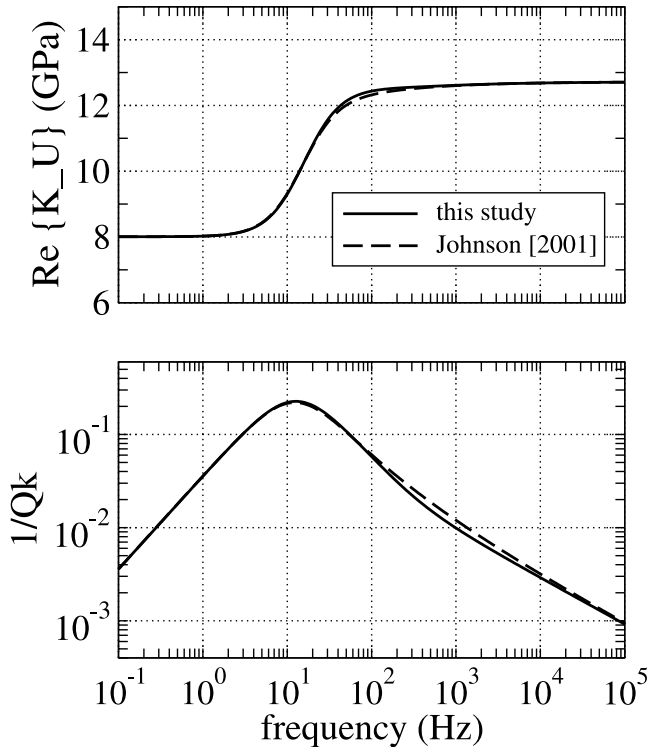

Figure 4. Undrained bulk modulus $K_U(\omega)$ in both the patchy saturation model presented in this article and the model of *Johnson* [2001]: (top) $\mathrm{Re}\{K_U\}$ and (bottom) $Q_K^{-1} = -\mathrm{Im}\{K_U\}/\mathrm{Re}\{K_U\}$. The physical model is 10 cm spherical air pockets embedded within a water-saturated region. The volume fraction of gas saturated rock is 3% in this example. The properties of the rock correspond to a 100 mdarcy consolidated sandstone.

[77] Figure 5 gives the P wave velocity and attenuation for a model in which the frame properties correspond to $k = 10$ mdarcy, $c = 15$, and $\phi = 0.15$. Phase 2 is saturated by air and is taken to be isolated spheres of radius $a = 1$ cm. Phase 1 is saturated with water. The volume fraction v_2 occupied by these 1 cm spheres of gas is as shown in Figure 5. Even tiny amounts of gas saturation yield rather large amounts of attenuation and dispersion; yet these predictions are consistent with the magnitudes of observed attenuation and dispersion in rocks.

4. Squirt Flow Model

[78] Laboratory samples of consolidated rock often have broken grain contacts and/or microcracks in the grains. Much of this damage occurs as the rock is brought from depth to the surface. Since diagenetic processes in a sedimentary basin tend to cement microcracks and grain

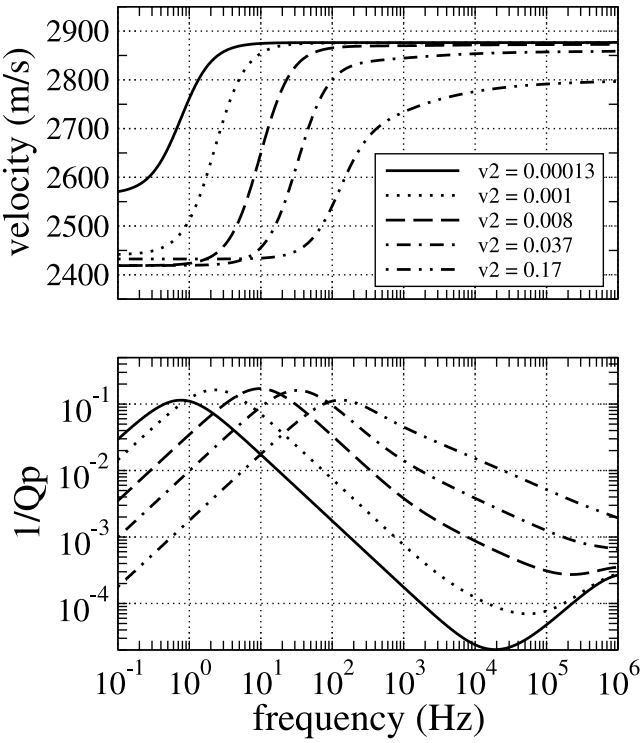

Figure 5. *P* wave velocity and attenuation of a sandstone saturated with water and containing small spherical pockets of gas having radius 1 cm and occupying a fraction of the volume v_2 as shown.

contacts, it is uncertain whether in situ rocks have significant numbers of open microcracks. Nonetheless, when such grain-scale damage is present, as it always is in laboratory rock samples at ambient pressures, the fluid pressure response in the microcracks will be greater than in the principal pore space when the rock is compressed by a *P* wave. The resulting flow from crack to pore is called "squirt flow" [e.g., *Mavko and Nur*, 1975].

[79] In the squirt model of *Dvorkin et al.* [1995], the grains of a porous material are themselves allowed to have porosity in the form of microcracks. The effect of each broken grain contact is taken as equivalent to a microcrack in a grain. The number of such microcracks per grain is thus limited by the coordination number of the packing and so the total porosity contribution coming from the grains is always negligible compared to the porosity of the main pore space.

[80] The grain space in the *Dvorkin et al.* [1995] model is taken to be a spatially uniform porous continuum. Dvorkin et al. provide an approximate analysis of their model in which the terms that are left out of the bulk modulus dispersion are as large as the dispersion itself. In this section, we use the double-porosity framework to analyze the *Dvorkin et al.* [1995] squirt model with the goal of obtaining exact results at both low and high frequencies. As in sections 2 and 3, our exact limits are approximately connected by a causal frequency function containing a relaxation frequency appropriate for a grain space of arbitrary geometry.

[81] Phase 1 is now defined to be the pure fluid within the main pore space of a sample and is characterized elastically by the single modulus K_f (fluid bulk modulus). Phase 2 is taken to be the porous (i.e., cracked) grains and characterized by the poroelastic constants K_2^d (the drained modulus of an isolated porous grain), α_2 (the Biot-Willis constant of an isolated grain), and B_2 (Skempton's coefficient of an isolated grain) as well as by a permeability k_2. The overall composite of porous grains (phase 2) packed together within the fluid (phase 1) has two distinct properties of its own that must be specified; an overall drained modulus K, and an overall permeability k associated with flow through the main pore space. The volume fractions occupied by each phase are again denoted v_i where $v_1 = \phi$ is the porosity associated with the main pore space.

[82] The theoretical approach is to again obtain the average fluid response in each of these two phases and then to make an effective Biot theory by saying that the fluid within the grains cannot communicate directly with the outside world; that is, the fluid in the grains can only communicate with the main pores. Equations (11)–(13) again define the effective poroelastic moduli in the squirt model and we need only determine the a_{ij} constants and internal transport coefficient $\gamma(\omega)$ that are appropriate to squirt.

4.1. Squirt a_{ij} Coefficients

[83] To obtain the a_{ij} coefficients in the squirt model, we first note that these coefficients are defined under conditions where $\dot{\zeta}_{\text{int}} = 0$ (no fluid passing between the porous grains and the principal pore space). Under these conditions, the rate of fluid depletion $\nabla \cdot \mathbf{q}_1$ of a sample (rate of fluid volume being extruded from the principal pore space via the exterior sample surface as normalized by the sample volume) is due to the difference between the rate of dilatation of the principal pore space (denoted here as $\dot{e}_1$) and the rate at which fluid in the pores is dilating $-\dot{\bar{p}}_{f1}/K_f$. If we also perform a volume average of equation (3) over the porous grain space and use the notation that $v_2\dot{e}_2 = \nabla \cdot (v_2\dot{\mathbf{u}}_2)$ we obtain the following three equations:

$$-\nabla \cdot \mathbf{q}_1 = v_1\dot{e}_1 + \frac{v_1}{K_f}\dot{\bar{p}}_{f1}, \tag{88}$$

$$-\nabla \cdot \mathbf{q}_2 = -\frac{v_2\alpha_2}{K_2^d}\dot{\bar{p}}_{c2} + \frac{v_2\alpha_2}{B_2K_2^d}\dot{\bar{p}}_{f2}, \tag{89}$$

$$-v_2\dot{e}_2 = \frac{v_2}{K_2^d}\dot{\bar{p}}_{c2} - \frac{v_2\alpha_2}{K_2^d}\dot{\bar{p}}_{f2}. \tag{90}$$

The macroscopic dilatation of interest is $\nabla \cdot \mathbf{v} = v_1\dot{e}_1 + v_2\dot{e}_2$. In order to obtain the macroscopic compressibility laws for the porous grain/principal pore space composite, we introduce linear response laws of the form

$$\dot{\bar{p}}_{c2} = a_1\dot{P}_c + a_2\dot{\bar{p}}_{f1} + a_3\dot{\bar{p}}_{f2} \tag{91}$$

$$\dot{e}_1 = b_1\dot{P}_c + b_2\dot{\bar{p}}_{f1} + b_3\dot{\bar{p}}_{f2}, \tag{92}$$

where the a_i and b_i must be found. We note immediately that from the definition $\bar{P}_c = v_1\bar{p}_{f1} + v_2\bar{p}_{c2}$ one has

$$0 = (1 - v_2a_1)\dot{P}_c - (v_1 + v_2a_2)\dot{\bar{p}}_{f1} - v_2a_3\dot{\bar{p}}_{f2}, \tag{93}$$

which must hold true for any variation of the independent pressure variables so that $a_1 = 1/v_2$, $a_2 = -v_1/v_2$, $a_3 = 0$.

[84] To obtain the b_i, we now combine the above into the macroscopic laws

$$-\nabla\cdot\mathbf{v}=\left[-v_1b_1+\frac{1}{K_2^d}\right]\dot{P}_c-\left[v_1b_2+\frac{v_1}{K_2^d}\right]\dot{\bar{p}}_{f1}-\left[v_1b_3+\frac{v_2\alpha_2}{K_2^d}\right]\dot{\bar{p}}_{f2}, \tag{94}$$

$$-\nabla\cdot\mathbf{q}_1=v_1b_1\dot{P}_c+\left[v_1b_2+\frac{v_1}{K_f}\right]\dot{\bar{p}}_{f1}+v_1b_3\dot{\bar{p}}_{f2}, \tag{95}$$

$$-\nabla\cdot\mathbf{q}_2=\frac{-\alpha_2}{K_2^d}\dot{P}_c+\frac{v_1\alpha_2}{K_2^d}\dot{\bar{p}}_{f1}+\frac{v_2\alpha_2}{K_2^dB_2}\dot{\bar{p}}_{f2} \tag{96}$$

and use the fact that the coefficients of the matrix must be symmetric ($a_{ij}=a_{ji}$). With $a_{11}=1/K$ corresponding to the overall drained frame modulus of the composite (to be independently specified), we obtain $v_1b_1=-(1/K-1/K_2^d)$, $v_1b_2=1/K-(1+v_1)/K_2^d$, and $b_3=\alpha_2/K_2^d$. The final a_{ij} coefficients are exactly

$$a_{11}=1/K, \tag{97}$$

$$a_{22}=1/K-(1+v_1)/K_2^d+v_1/K_f, \tag{98}$$

$$a_{33}=\frac{v_2\alpha_2}{B_2K_2^d}, \tag{99}$$

$$a_{12}=-1/K+1/K_2^d, \tag{100}$$

$$a_{13}=-\alpha_2/K_2^d, \tag{101}$$

$$a_{23}=v_1\alpha_2/K_2^d. \tag{102}$$

Reasonable models for K and K_2^d will be discussed shortly.

4.2. Squirt Transport

[85] We next must obtain the coefficient $\gamma(\omega)$ in the mesoscopic transport law $-i\omega\,\zeta_{\text{int}}=\gamma(\omega)\,(\bar{p}_{f1}-\bar{p}_{f2})$. Again, the approach is to first obtain the limiting behavior at low and high frequencies and then to connect the two limits by a simple function.

[86] The fluid response in phase 1 (the principal pore space) is governed by the Navier-Stokes equation $-\nabla p_{f1}+\eta\nabla^2\mathbf{v}_1=-i\omega\rho_f\mathbf{v}_1$ and the compressibility law $K_f\nabla\cdot\mathbf{v}_1=i\omega p_{f1}$ where $\mathbf{v}_1$ is the local fluid velocity in the pores. Since for all frequencies of interest we have that $\omega\ll K_f/\eta$ (note that $K_f/\eta\approx10^{12}$ s^{-1} for liquids and 10^{10} s^{-1} for gases), the fluid pressure in phase 1 is governed by the wave equation

$$\nabla^2p_{f1}+\omega^2\frac{\rho_f}{K_f}p_{f1}=0, \tag{103}$$

and since the acoustic wavelength in the fluid is always much greater than the grain sizes, the fluid pressure in the principal pore space satisfies $p_{f1}(\mathbf{r})=\bar{p}_{f1}$ (a spatial constant) at all frequencies.

[87] The focus, then, is on determining the flow and fluid pressure within the cracked grains (phase 2) that is governed by the local porous continuum laws $\mathbf{Q}_2=-(k_2/\eta)\nabla p_{f2}$ and

$$\frac{k_2}{\eta}\nabla^2p_{f2}+i\omega\frac{\alpha_2}{K_2^dB_2}p_{f2}=-i\omega\frac{\alpha_2}{K_2^d}p_{c2}, \tag{104}$$

where $p_{c2}=-K_2^d\nabla\cdot\mathbf{u}_2+\alpha_2p_{f2}$. This deformation and pressure change is excited by applying a uniform normal stress $-\Delta P\mathbf{n}$ to the surface of the averaging volume with the fluid pressure satisfying the boundary conditions $\mathbf{n}\cdot\nabla p_{f2}(\mathbf{r})=0$ on ∂E_2 and $p_{f2}(\mathbf{r})=\bar{p}_{f1}$ on $\partial\Omega_{12}$.

4.2.1. Low-Frequency Limit of $\gamma(\omega)$

[88] The fluid pressure and confining pressure in the grains can again be developed as a power series in $-i\omega$ (as in equations (67)–(68)). The zero-order response corresponds to the static limit in which the fluid pressure is everywhere the same and given by $p_{f2}^{(0)}=\bar{p}_{f1}=B_o\Delta P$ with $B_o=-(a_{12}+a_{13})/(a_{22}+2a_{23}+a_{33})$ and with the a_{ij} as given by equations (97)–(102). The detailed result for B_o can be expressed

$$\frac{1/K-(1-\alpha_2)/K_2^d}{B_o}=\frac{1}{K}-\frac{(1-\alpha_2)}{K_2^d}+v_1\left[\frac{1}{K_f}-\frac{(1-\alpha_2)}{K_2^d}\right]+v_2\frac{\alpha_2}{K_2^d}\left[\frac{1}{B_2}-1\right], \tag{105}$$

which reduces to the standard Gassmann expression given in Appendix A (with a total porosity given by $v_1+\phi_2v_2$), when B_2 and α_2 are themselves given by the Gassmann expressions. In this same zero-order limit, the undrained bulk modulus is defined as $1/K_o^u=a_{11}+(a_{12}+a_{13})B_o$, which also reduces to the standard Gassmann expression, when B_2 and α_2 are themselves given by Gassmann expressions.

[89] The leading order in $-i\omega$ correction to uniform fluid pressure is thus governed by the problem

$$\nabla^2p_{f2}^{(1)}=\frac{\eta\alpha_2}{k_2K_2^d}p_{c2}^{(0)}, \tag{106}$$

$$\mathbf{n}\cdot\nabla p_{f2}^{(1)}=0\quad\text{on}\quad\partial E_2, \tag{107}$$

$$p_{f2}^{(1)}=0\quad\text{on}\quad\partial\Omega_{12}. \tag{108}$$

Here, $p_{c2}^{(0)}$ is the local confining pressure in the grain space in the static limit that can be written $p_{c2}^{(0)}(\mathbf{r})=\bar{p}_{c2}^{(0)}+\delta P(\mathbf{r})$. The average static confining pressure throughout the grains is determined from equation (84) with $P_c=\Delta P$ and $p_{f2}=p_{f1}=B_o\Delta P$ to yield

$$\bar{p}_{c2}^{(0)}=\frac{(1-v_1B_o)}{v_2}\Delta P. \tag{109}$$

The deviations $\delta P(\mathbf{r})$ thus integrate by volume to zero $\overline{\delta P}=0$ and are formally defined

$$\delta P(\mathbf{r})=-\left(\frac{1-(v_1+v_2\alpha_2)B_o}{v_2}\right)\Delta P-\frac{K_2^d}{\alpha_2}\nabla\cdot\mathbf{u}^{(0)}(\mathbf{r}). \tag{110}$$

The local perturbations $\delta P(\mathbf{r})$ are thus highly sensitive to the detailed nature of the grain packing and grain geometry. Fortunately, the details of these perturbations do not play an important role in the theory.

[90] The fluid pressure in the grains is now written in the scaled form

$$p_{f2}^{(1)}(\mathbf{r})=-\frac{\eta\alpha_2(1-v_1B_o)}{v_2k_2K_s^d}\Delta P\,\Phi(\mathbf{r}), \tag{111}$$

where the potential $\Phi(\mathbf{r})$ is independent of ΔP and is a solution of the elliptic problem

$$\nabla^2\Phi(\mathbf{r}) = -1 - \frac{v_2}{1-v_1B_o}\frac{\delta P(\mathbf{r})}{\Delta P}, \tag{112}$$

$$\mathbf{n}\cdot\nabla\Phi = 0 \quad \text{on} \quad \partial E_2, \tag{113}$$

$$\Phi = 0 \quad \text{on} \quad \partial\Omega_{12}. \tag{114}$$

To leading order in $-i\omega$, an average of equation (111) gives

$$\begin{aligned}\overline{p}_{f1} - \overline{p}_{f2} &= i\omega\overline{p}_{f2}^{(1)} + O(\omega^2)\\ &= -i\omega\frac{\eta\alpha_2(1-v_1B_o)}{v_2k_2K_s^d}L_2^2\Delta P + O(\omega^2),\end{aligned} \tag{115}$$

where the squared length L_2^2 is defined

$$L_2^2 = \overline{\Phi} = \overline{\Phi}_o\left[1 + \frac{v_2}{1-v_1B_o}\frac{\overline{\Phi_o\delta P}}{\overline{\Phi}_o\Delta P}\right], \tag{116}$$

with overlines denoting volume averages over the grain space and with the potential Φ_o defined as the solution of

$$\nabla^2\Phi_o = -1, \tag{117}$$

$$\mathbf{n}\cdot\nabla\Phi_o = 0 \quad \text{on} \quad \partial E_2, \tag{118}$$

$$\Phi_o = 0 \quad \text{on} \quad \partial\Omega_{12}. \tag{119}$$

Although it is not generally true that $\overline{\Phi_o\delta P} = 0$ for all grain geometries, we nevertheless expect this integral to be small in general because Φ_o is a smooth function and $\overline{\delta P} = 0$. The local perturbations in the static confining pressure $\delta P(\mathbf{r})$ require a solution of the static displacements throughout the entire grain space, a daunting numerical task. Whenever the length L_2 needs to be estimated, such as in the numerical results that follow, our approach is simply to use the reasonable approximation that $L_2^2 = \bar{\Phi}_o$.

[91] Last, from the definition ζ_{int} of the internal transfer we have that to leading order in $-i\omega$:

$$\begin{aligned}-i\omega\zeta_{\text{int}} &= \frac{i\omega k_2}{V\eta}\int_{\partial\Omega_{12}}\mathbf{n}\cdot\nabla p_{f2}^{(1)}\,dS\\ &= \frac{-i\omega k_2}{V\eta}\int_{\Omega_2}\nabla^2 p_{f2}^{(1)}\,dV = -i\omega\frac{\alpha_2}{K_2^d}v_2\overline{p}_{c2}^{(0)}\\ &= \frac{v_2k_2}{\eta L_2^2}\left(\overline{p}_{f1} - \overline{p}_{f2}\right),\end{aligned} \tag{120}$$

where equation (120) follows from equations (109) and (115). The desired result is thus $\lim_{\omega\to 0}\gamma(\omega) = \gamma_{sq} = v_2k_2/(\eta L_2^2)$.

4.2.2. High-Frequency Limit of $\gamma(\omega)$

[92] In the extreme high-frequency limit, the fluid has no time to escape in significant amounts from the porous grains (phase 2) and enter the main pore space (phase 1). As such, the fluid pressure distribution in each phase is reasonably modeled as

$$p_{f1}(\mathbf{r}) = B_1^\infty\Delta P \tag{121}$$

$$p_{f2}(\mathbf{r}) = B_2^\infty\Delta P + C_2\Delta P e^{-i^{3/2}\sqrt{\omega/D_2}\,x}, \tag{122}$$

where x is again a local coordinate measuring distance normal to the interface $\partial\Omega_{12}$ and where D_2 is the fluid pressure diffusivity within the porous grains that is given by $D_2 = k_2K_2^dB_2/(\eta\alpha_2)$. In reality, the local confining pressure $p_{c2}(\mathbf{r})$ throughout the grains has spatial fluctuations about the average value and we have made the approximation that the average fluid pressure throughout the grain space is $B_2p_{c2}(\mathbf{r}) \approx B_2^\infty\Delta P$. It is easy to demonstrate that under undrained and unrelaxed conditions,

$$B_1^\infty = \frac{a_{13}a_{23} - a_{33}a_{12}}{a_{22}a_{33} - a_{23}^2} \tag{123}$$

$$B_2^\infty = \frac{a_{12}a_{23} - a_{22}a_{13}}{a_{22}a_{33} - a_{23}^2}. \tag{124}$$

However, since these B_i^∞ do not appear in the final result, they will not be algebraically developed.

[93] The continuity of fluid pressure $p_{f2} = p_{f1}$ along $\partial\Omega_{12}$ ($x = 0$) requires that $C_2 = B_1^\infty - B_2^\infty$. The definition of ζ_{int} may now be used to write

$$\begin{aligned}-i\omega\zeta_{\text{int}} &= \frac{1}{V}\int_{\partial\Omega_{12}}\frac{k_2}{\eta}\frac{\partial p_2}{\partial x}\\ &= \frac{k_2}{\eta}i^{3/2}\sqrt{\frac{\omega}{D_2}}\frac{S}{V}\left(B_1^\infty - B_2^\infty\right)\Delta P\\ &= i^{3/2}\sqrt{\omega}\sqrt{\frac{k_2\alpha_2}{\eta B_2K_2^d}}\frac{S}{V}\left(\overline{p}_{f1} - \overline{p}_{f2}\right),\end{aligned} \tag{125}$$

where we have used, to leading order in the high-frequency limit, $\bar{p}_{f1} - \bar{p}_{f2} = (B_1^\infty - B_2^\infty)\Delta P$. The desired result is then

$$\gamma(\omega) \sim \frac{S}{V}\sqrt{\frac{-i\omega k_2\alpha_2}{\eta B_2K_s^d}} \tag{126}$$

as $\omega \to \infty$.

4.2.3. Full Model for $\gamma(\omega)$

[94] The high- and low-frequency limits are again causally connected via the simple function

$$\gamma(\omega) = \gamma_{sq}\sqrt{1 - \frac{i\omega}{\omega_{sq}}}, \tag{127}$$

but now the parameters are defined as

$$\gamma_{sq} = \frac{v_2k_2}{\eta L_2^2} \tag{128}$$

$$\omega_{sq} = \frac{B_2K_2^d}{\eta\alpha_2}\frac{k_2}{L_2^2}\left(\frac{v_2V/S}{L_2}\right)^2. \tag{129}$$

4.3. Squirt Flow Modeling Choices

[95] To make numerical predictions of attenuation and dispersion, models must be proposed for the phase 2 (porous grain) parameters.

[96] If the grains are modeled as spheres of radius R, the fluid pressure gradient length within the grains can be estimated as $L_2 = R/\sqrt{15}$ and the volume to surface ratio as $V/S = R/(3v_2)$. The grain porosity is assumed to be in the form of microcracks and so it is natural to define an effective aperture h for these cracks. If the cracks have an average effective radius of R/N_R (where N_R is roughly 2 or 3) and if there are on average N_c cracks per grain (where N_c is also roughly 2 or 3), then the permeability and porosity of the grains are reasonably modeled as

$$\begin{aligned}\phi_2 &= \frac{3N_c}{4N_R^2}\frac{h}{R}\\ k_2 &= \phi_2h^2/12,\end{aligned} \tag{130}$$

where ϕ_2 is the fracture porosity within the porous grains. The dimensionless parameters k_2/L_2^2 and $(v_2V/S)/L_2$ required in the expressions for γ_{sq} and ω_{sq} are now given by

$$\frac{k_2}{L_2^2} = \frac{15N_c}{16N_R^2}\left(\frac{h}{R}\right)^3$$
$$\left(\frac{v_2V/S}{L_2}\right)^2 = \frac{5}{3}. \tag{131}$$

The normalized fracture aperture h/R is the key parameter in the squirt model.

[97] The drained grain modulus K_2^d is necessarily a function of the crack porosity ϕ_2 (and therefore h/R). Real crack surfaces have micron (and smaller) scale asperities present upon them. If effective stress is applied in order to make the normalized aperture h/R smaller (so that, for example, the peak in squirt attenuation lies in the seismic band), new contacts are created that make the crack stronger. In the limit as $h/R \rightarrow 0$ (large effective stress), the cracks are no longer present and $K_2^d \rightarrow K_s$, where K_s is the mineral modulus of the grain.

[98] Many models for such stiffening could be proposed. We intentionally make a conservative estimate here in proposing a simple linear porosity dependence $K_2^d = K_s(1 - \sigma\phi_2)$, where σ is a fixed constant determined from fitting ultrasonic attenuation data. Effective medium theories [see, e.g., *Berryman et al.*, 2002] predict that σ should be inversely proportional to the aspect ratios of the cracks present. As a crack closes and asperities are brought into contact, there is naturally a decrease in ϕ_2, but there should also be a decrease in σ due to the fact that the remaining crack porosity becomes more equant as new asperities come into contact. Taking σ to be constant as crack porosity decreases is thus a minimalist estimate for how the drained modulus increases.

[99] Thus the porous grain elastic properties are taken to be

$$K_2^d = K_s(1 - \sigma\phi_2), \tag{132}$$

$$\alpha_2 = 1 - K_2^d/K_s, \tag{133}$$

$$\frac{1}{B_2} = 1 + \phi_2\frac{K_2^d}{K_f}\left(\frac{1 - K_f/K_s}{1 - K_2^d/K_s}\right), \tag{134}$$

where we have used the Gassmann fluid substitution relations for α_2 and B_2. The overall drained modulus K of the collection of porous (cracked) grains can be modeled, for example, as

$$K = \frac{K_2^d(1 - v_1)}{1 + cv_1}, \tag{135}$$

which is the same drained modulus model as given in Appendix A but with the solid grain modulus K_s replaced by the cracked grain modulus K_2^d.

4.4. Numerical Examples

[100] In Figure 6 we plot the P wave attenuation predicted using the above model when the overall grain packing corresponds to a consolidated sandstone ($v_1 = 0.2$ and $c = 5$) having a permeability of 10 mdarcy. For the grain properties, we take $\sigma = 0.8/(5 \times 10^{-3})$, $3N_c/(4N_R^2) = 1$, and $K_s = 38$ GPa (quartz) as fixed constants. This σ value was chosen so that there would be a significant peak in attenuation at ultrasonic frequencies and is taken to be the same for all values of h/R. The various curves can be thought of as being due to the application of effective stress. The peak in Q^{-1} near 1 MHz that is invariant to h/R is the one due to the macroscopic Biot loss (fluid pressure equilibration at the scale of the wavelength). The peak that shifts with h/R is the one due to the squirt flow.

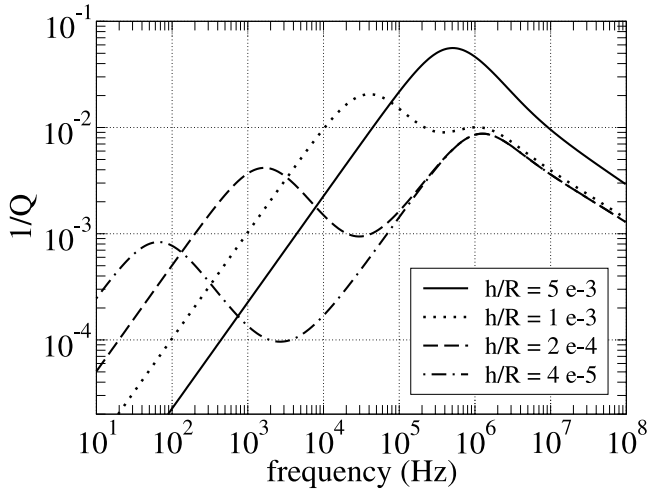

Figure 6. Squirt flow model of P wave attenuation when the grains are modeled as being spherical of radius R and containing microcracks having effective apertures h. The overall drained modulus of the rock corresponds to a consolidated sandstone.

[101] Figure 6 indicates that although the squirt mechanism is probably operative and perhaps even dominant at ultrasonic frequencies, it does not seem to be involved in explaining the observed levels of intrinsic attenuation in exploration work. For real cracks inside of real grains, the σ value will diminish with effective stress (i.e., with h/R), so that the effects of squirt in the seismic band are likely to be even less than shown in Figure 6.

[102] We next introduce the grain parameters k_2, ϕ_2, and K_2^d as modeled here along with the same overall drained modulus K into the equations of *Dvorkin et al.* [1995] and compare their results to our own when $h/R = 5 \times 10^{-3}$ (Figure 7). *Dvorkin et al.* [1995] have made a series of approximations in their analysis (starting with equation (3) in their paper) in which the error introduced is often as large as the dispersion being modeled. Figure 7 quantifies this error since our analysis of their model, at least in the limits of both low and high frequencies, is exact.

5. Conclusions

[103] Models for three different P wave attenuation mechanisms were derived using a single theoretical framework. The resulting models differ only in the values of the a_{ij} constants and in the values of the parameters contributing to the mesoscopic transport coefficient $\gamma(\omega)$. These three

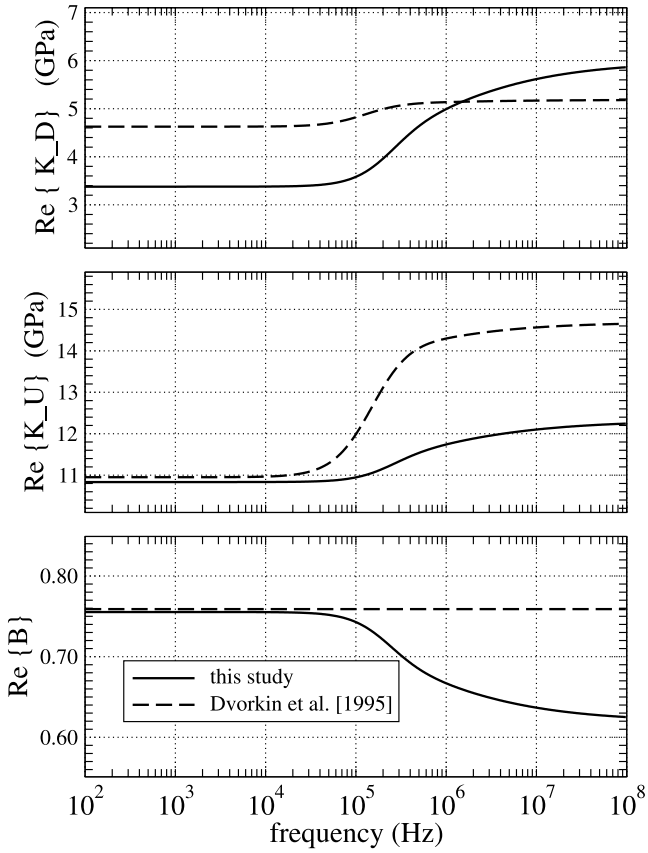

Figure 7. Dispersion (top) in the real parts of the drained bulk modulus K_D (ω), (middle) the undrained bulk modulus K_U(ω), and (bottom) the Skempton's coefficient B(ω) as determined both in the present study and by *Dvorkin et al.* [1995]. The plots were all generated with $h/R = 5 \times 10^{-3}$. Both theories use identically the same input parameters and are treating identically the same model. The present study may be considered exact in both the low- and high-frequency limits of the model.

models correspond to (1) mesoscopic-scale heterogeneity in the frame moduli ("double porosity"), (2) mesoscopic-scale heterogeneity in the fluid type ("patchy saturation"), and (3) grain-scale heterogeneity due to microcracks in the grains ("squirt"). In all three models, the amount of attenuation is controlled principally by the contrast of elastic compressibility among the constituents along with the assumed mesoscopic geometry. In the double-porosity model, it is necessary that the embedded phase have an elongated or squashed form and that the contrast between the frame bulk modulus of the two porous phases is strong in order for the mesoscopic loss to be significant. In the patchy saturation model, the contrast in the fluid bulk modulus must be strong (immiscible patches of different fluids that have nearly identical bulk moduli would not produce much attenuation), while in the squirt model, it is the contrast between the drained modulus of an isolated cracked grain and that of the entire packing of grains that controls the amount of attenuation.

[104] Putting in thin lenses of unconsolidated sand grains into an otherwise consolidated sandstone can produce attenuation in the seismic band that is comparable to what is measured in the field even when the embedded phase represents only a small amount of the total volume (<1% volume fractions). Such a model might correspond to a jointed sandstone. Since mesoscopic-scale heterogeneity is rather ubiquitous throughout the earth's crust, it seems reasonable to suppose that this mechanism may be responsible for most of the attenuation observed in seismograms. The squirt mechanism produces a great deal of attenuation at the ultrasonic frequencies used in laboratory measurements, but has trouble explaining attenuation in the seismic band. This result is important for some applications of the theory because the rate at which the mesoscopic-scale fluid pressure equilibrates is a strong function of the permeability of the porous material. The rate at which microcracks equilibrate with the main pores in squirt flow is not permeability-dependent. This leaves open the possibility of extracting permeability information from the frequency dependence of seismically measured Q.

Appendix A: Constituent Properties

[105] In order to use the unified double-porosity framework of the present paper, it is convenient to have models for the various porous continuum constituent properties.

[106] For unconsolidated sands and soils, the frame moduli (drained bulk modulus K^d and shear modulus G) are well modeled using the following variant of the *Walton* [1987] theory (see *Pride* [2003] for details)

$$K^d = \frac{1}{6}\left[\frac{4(1-\phi_o)^2 n_o^2 P_o}{\pi^4 C_s^2}\right]^{1/3} \frac{(P_e/P_o)^{1/2}}{\left\{1+[16P_e/(9P_o)]^4\right\}^{1/24}} \quad \text{(A1)}$$

$$G = 3K^d/5, \quad \text{(A2)}$$

where P_e is the effective overburden pressure (e.g., $P_e = (1-\phi)(\rho_s - \rho_f)\, gh$, where g is gravity and h is overburden thickness) and P_o is the effective pressure at which all grain-to-grain contacts are established. For $P_e < P_o$, the coordination number n (average number of grain contacts per grain) is increasing as $(P_e/P_o)^{1/2}$. For $P_e > P_o$, the coordination number remains constant $n = n_o$. The parameter P_o is commonly on the order of 10 MPa. As $P_o \to 0$, the *Walton* [1987] result is obtained (all contacts in place starting from $P_e = 0$). The porosity of the grain pack is ϕ_o and the compliance parameter C_s are defined

$$C_s = \frac{1}{4\pi}\left(\frac{1}{G_s} + \frac{1}{K_s + G_s/3}\right) \quad \text{(A3)}$$

where K_s and G_s are the mineral moduli of the grains. For unimodal grain-size distributions and random grain packs, one typically has $0.32 < \phi_o < 0.36$ and $8 < n_o < 11$. In the numerical examples we use $\phi_o = 0.36$, $n_o = 9$, and $P_o = 10$ MPa.

[107] For consolidated sandstones, the frame moduli are modelled in the present paper as (see *Pride* [2003] for details)

$$K^d = K_s \frac{1-\phi}{1+c\phi}, \quad \text{(A4)}$$

$$G = G_s \frac{1-\phi}{1+3c\phi/2}. \quad \text{(A5)}$$

The consolidation parameter c represents the degree of consolidation between the grains and lies in the approximate range $2 < c < 20$ for sandstones. If it is necessary to use a c greater than say 20 or 30, then it is probably better to use the modified Walton theory.

[108] The undrained moduli K^u and B are conveniently and exactly modeled using the *Gassmann* [1951] theory whenever the grains are isotropic and composed of a single mineral. The results are

$$B = \frac{1/K^d - 1/K_s}{1/K^d - 1/K_s + \phi\left(1/K_f - 1/K_s\right)} \tag{A6}$$

$$K^u = \frac{K^d}{1 - B(1 - K^d/K_s)}, \tag{A7}$$

from which the Biot-Willis constant α may be determined to be $\alpha = 1 - K^d/K_s$. These Gassmann results are often called the ''fluid substitution'' relations.

[109] The dynamic permeability $k(\omega)$ as modeled by *Johnson et al.* [1987] is

$$\frac{k(\omega)}{k_o} = \left[\sqrt{1 - i\frac{4}{n_J}\frac{\omega}{\omega_c}} - i\frac{\omega}{\omega_c}\right]^{-1}, \tag{A8}$$

where the relaxation frequency ω_c, which controls the frequency at which viscous boundary layers first develop, is given by

$$\omega_c = \frac{\eta}{\rho_f F k_o}. \tag{A9}$$

Here, F is exactly the electrical formation factor when grain surface electrical conduction is not important and is conveniently (though crudely) modeled using Archie's law $F = \phi^{-m}$. The cementation exponent m is related to the distribution of grain shapes (or pore topology) in the sample and is generally close to 3/2 in clean sands, close to 2 in shaly sands, and close to 1 in rocks having fracture porosity (indeed, a reasonable model is $m = 3/2 + 1/c$). In the numerical modeling, the parameter n_J is, for convenience, taken to be 8 (cylinder model of the pore space).

[110] **Acknowledgments.** The work of S.R.P. was supported by the Director, Office of Science, Office of Basic Energy Sciences, of the U.S. Department of Energy under contract DE-AC03-76SF00098. The work of J.G.B. was performed under the auspices of the U.S. Department of Energy under contract W-7405-ENG-48 and supported specifically by the Geosciences Research Program of the DOE Office of Basic Energy Sciences, Division of Chemical Sciences, Geosciences and Biosciences. Work of J.G.B. also supported in part by the Stanford Exploration Project, while on sabbatical visiting the Geophysics Department at Stanford University. All three authors would like to thank the Associate Editor Jack Dvorkin and the two referees for having made useful suggestions that improved the paper.

References

Berryman, J. G. (1988), Seismic wave attenuation in fluid-saturated porous media, *Pure Appl. Geophys.*, *128*, 423–432.

Berryman, J. G., and G. W. Milton (1991), Exact results for generalized Gassmann's equations in composite porous media with two constituents, *Geophysics*, *56*, 1950–1960.

Berryman, J. G., and H. F. Wang (1995), The elastic coefficients of double-porosity models for fluid transport in jointed rock, *J. Geophys. Res.*, *100*, 24,611–24,627.

Berryman, J. G., and H. F. Wang (2000), Elastic wave propagation and attenuation in a double-porosity dual-permability medium, *Int. J. Rock Mech. Min. Sci.*, *37*, 63–78.

Berryman, J. G., S. R. Pride, and H. F. Wang (2002), A differential scheme for elastic properties of rocks with dry or saturated cracks, *Geophys. J. Int.*, *151*, 597–611.

Biot, M. A. (1956a), Theory of propagation of elastic waves in a fluid-saturated porous solid. I. Low-frequency range, *J. Acoust. Soc. Am.*, *28*, 168–178.

Biot, M. A. (1956b), Theory of propagation of elastic waves in a fluid-saturated porous solid. II. Higher frequency range, *J. Acoust. Soc. Am.*, *28*, 179–191.

Biot, M. A. (1962), Mechanics of deformation and acoustic propagation in porous media, *J. Appl. Phys.*, *33*, 1482–1498.

Biot, M. A., and D. G. Willis (1957), The elastic coefficients of the theory of consolidation, *J. Appl. Mech.*, *24*, 594–601.

Bruggeman, D. A. G. (1935), Berechnung verschiedener physikalischer Konstanten von heterogenen Substanzen, *Ann. Phys. Leipzig*, *24*, 636–679.

Budiansky, B., and R. J. O'Connell (1976), Elastic moduli of a cracked solid, *Int. J. Solids Struct.*, *12*, 81–97.

Cadoret, T., G. Mavko, and B. Zinszner (1998), Fluid distribution effect on sonic attenuation in partially saturated limestones, *Geophysics*, *63*, 154–160.

deGroot, S. R., and P. Mazur (1984), *Non-equilibrium Thermodynamics*, Dover, Mineola, N. Y.

Dutta, N. C., and H. Odé (1979a), Attenuation and dispersion of compressional waves in fluid-filled porous rocks with partial gas saturation (White model)—part I: Biot theory, *Geophysics*, *44*, 1777–1788.

Dutta, N. C., and H. Odé (1979b), Attenuation and dispersion of compressional waves in fluid-filled porous rocks with partial gas saturation (White model)—part II: Results, *Geophysics*, *44*, 789–805.

Dutta, N. C., and A. J. Seriff (1979), On White's model of attenuation in rocks with partial gas saturation, *Geophysics*, *44*, 1806–1812.

Dvorkin, J., G. Mavko, and A. Nur (1995), Squirt flow in fully saturated rocks, *Geophysics*, *60*, 97–107.

Gassmann, F. (1951), Über die Elastizität poröser Medien, *Vierteljahrsschr. Naturforsch. Ges. Zuerich*, *96*, 1–23.

Gelinsky, S., and S. A. Shapiro (1997), Dynamic-equivalent medium approach for thinly layered saturated sediments, *Geophys. J. Int.*, *128*, F1–F4.

Gurevich, B., and S. L. Lopatnikov (1995), Velocity and attenuation of elastic waves in finely layered porous rocks, *Geophys. J. Int.*, *121*, 933–947.

Hashin, Z. (1962), The elastic moduli of heterogeneous materials, *J. Appl. Mech.*, *29*, 143–150.

Hashin, Z., and S. Shtrikman (1963), A variational approach to the theory of the elastic behavior of multiphase materials, *J. Mech. Phys. Solids*, *11*, 127–140.

Hill, R. (1963), Elastic properties of reinforced solids: Some theoretical principles, *J. Mech. Phys. Solids*, *11*, 357–372.

Johnson, D. L. (2001), Theory of frequency dependent acoustics in patchy-saturated porous media, *J. Acoust. Soc. Am.*, *110*, 682–694.

Johnson, D. L., J. Koplik, and R. Dashen (1987), Theory of dynamic permeability and tortuosity in fluid-saturated porous media, *J. Fluid Mech.*, *176*, 379–402.

Knight, R., J. Dvorkin, and A. Nur (1998), Acoustic signatures of partial saturation, *Geophysics*, *63*, 132–138.

Mavko, G., and A. Nur (1975), Melt squirt in the asthenosphere, *J. Geophys. Res.*, *80*, 1444–1448.

Mavko, G., and A. Nur (1979), Wave attenuation in partially saturated rocks, *Geophysics*, *44*, 161–178.

Murphy, W. F., III (1982), Effects of partial water saturation on attenuation in Massilon sandstone and Vycor porous-glass, *J. Acoust. Soc. Am.*, *71*, 1458–1468.

Murphy, W. F., III (1984), Acoustic measures of partial gas saturation in tight sandstones, *J. Geophys. Res.*, *89*, 1549–1559.

Nagy, P. B., and G. Blaho (1994), Experimental measurements of surface stiffness on water-saturated porous solids, *J. Acoust. Soc. Am.*, *95*, 828–835.

Nagy, P. B., and A. H. Nayfeh (1995), Generalized formula for the surface stiffness of fluid-saturated porous media containing parallel pore channels, *Appl. Phys. Lett.*, *67*, 1827–1829.

Norris, A. N. (1993), Low-frequency dispersion and attenuation in partially saturated rocks, *J. Acoust. Soc. Am.*, *94*, 359–370.

O'Connell, R. J., and B. Budiansky (1977), Viscoelastic properties of fluid-saturated cracked solids, *J. Geophys. Res.*, *82*, 5719–5735.

Pride, S. R. (2003), Relationships between seismic and hydrological properties, in *Hydrogeophysics*, edited by Y. Rubin and S. Hubbard, pp. 1–31, Kluwer Acad., New York.

Pride, S. R., and J. G. Berryman (2003a), Linear dynamics of double-porosity and dual-permeability materials. I. Governing equations and acoustic attenuation, *Phys. Rev. E*, *68*, 036603.

Pride, S. R., and J. G. Berryman (2003b), Linear dynamics of double-porosity and dual-permeability materials. II. Fluid transport equations, *Phys. Rev. E*, *68*, 036604.

Pride, S. R., and E. G. Flekkoy (1999), Two-phase flow through porous media in the fixed-contact-line regime, *Phys. Rev. E*, *60*, 4285–4299.

Quan, Y., and J. M. Harris (1997), Seismic attenuation tomography using the frequency shift method, *Geophysics*, *62*, 895–905.

Roscoe, R. (1973), Isotropic composites with elastic or viscoelastic phases: General bounds for the moduli and solutions for special geometries, *Rheol. Acta*, *12*, 404–411.

Sams, M. S., J. P. Neep, M. H. Worthington, and M. S. King (1997), The measurement of velocity dispersion and frequency-dependent intrinsic attenuation in sedimentary rocks, *Geophysics*, *62*, 1456–1464.

Sato, H., and M. Fehler (1998), *Seismic wave propagation and scattering in the heterogeneous earth*, Springer-Verlag, New York.

Skempton, A. W. (1954), The pore-pressure coefficients A and B, *Geotechnique*, *4*, 143–147.

Thompson, A. H., A. J. Katz, and C. E. Krohn (1987), The microgeometry and transport properties of sedimentary rock, *Adv. Phys.*, *36*, 625–694.

Tserkovnyak, Y., and D. L. Johnson (2003), Capillary forces in the acoustics of patchy-saturated porous media, *J. Acoust. Soc. Am.*, *114*, 2596–2606.

Walton, K. (1987), The effective elastic moduli of a random packing of spheres, *J. Mech. Phys. Solids*, *35*, 213–226.

White, J. E. (1975), Computed seismic speeds and attenuation in rocks with partial gas saturation, *Geophysics*, *40*, 224–232.

White, J. E., N. G. Mikhaylova, and F. M. Lyakhovitsky (1975), Low-frequency seismic waves in fluid-saturated layered rocks, *Izvestija Academy of Sciences USSR, Phys. Solid Earth*, *11*, 654–659.

Williams, K. L., D. R. Jackson, E. I. Thorsos, D. Tang, and S. G. Schock (2002), Comparison of sound speed and attenuation measured in a sandy sediment to predictions based on the Biot theory of porous media, *IEEE J. Ocean. Eng.*, *27*, 413–428.

Wu, R. S., and K. Aki (1988), Multiple scattering and energy transfer of seismic waves: separation of scattering effect from intrinsic attenuation. II. Application of the theory to Hindu Kush region, *Pure Appl. Geophys.*, *128*, 49–80.

J. G. Berryman, University of California, Lawrence Livermore National Laboratory, P. O. Box 808 L-200, USA. (berryman1@llnl.gov)

J. M. Harris, Department of Geophysics, Stanford University, Stanford, CA 94305, USA. (harris@pangea.stanford.edu)

S. R. Pride, Lawrence Berkeley National Laboratory, Earth Sciences Division, 1 Cyclotron Road MS 90-1116, Berkeley, CA 94720, USA. (srpride@lbl.gov)